Thin–Walled Structures 204 (2024) 112268

Contents lists available at ScienceDirect

Thin-Walled Structures

journal homepage: www.elsevier.com/locate/tws

Full length article

Behaviour, finite element modelling and design of flanged cruciform section steel columns

Ruikai Dai [a], Behnam Behzadi-Sofiani [a], Spiridione Buhagiar [b], M. Ahmer Wadee [a,*], Leroy Gardner [a]

[a] Department of Civil and Environmental Engineering, Imperial College London, London SW7 2AZ, United Kingdom
[b] Department of Civil and Structural Engineering, University of Malta, MSD 2080, Malta

ARTICLE INFO

Keywords:
Flanged cruciform section
Cruciform columns
Torsional buckling
Post-buckling stability
Torsional strength
EC3 design approach

ABSTRACT

A study into the mechanical behaviour and design of flanged cruciform section steel members subjected to axial compression is presented herein. The mechanical behaviour of flanged cruciform section columns is first described, with particular emphasis on the newly developed approach for determining the elastic local buckling load for full flanged cruciform cross-sections. Existing experimental data on flanged cruciform section steel columns collected from the literature are then employed to validate numerical models developed within the finite element package ABAQUS. A comprehensive parametric study is subsequently conducted that encompasses a broad spectrum of cross-sectional geometries and global slenderness values. The mechanical behaviour and ultimate resistance of flanged cruciform section columns are shown to be dependent on not only the global slenderness, but also on the ratio of the elastic torsional to flexural buckling loads. The existing experimental data alongside the numerical parametric study results are employed to evaluate the resistance predictions provided in the current Eurocode 3 design codes, revealing a high degree of conservatism. Finally, a new design approach for flanged cruciform section columns, suitable for incorporation into future revisions of Eurocode 3, is proposed which provides significantly improved accuracy and consistency in resistance predictions compared with the current provisions. A reliability analysis of the proposed design approach is conducted in accordance with the EN 1990 procedure, resulting in a recommended partial safety factor $\gamma_{M1} = 1.0$.

1. Introduction

Flanged cruciform section members are compound structural components that are typically fabricated with two identical hot-rolled I-section members with one being cut into halves along its longitudinal centreline and then both halves being fillet welded along the longitudinal centreline of the other I-section member, as illustrated in Fig. 1. In engineering practice, flanged cruciform section members are widely employed as columns subjected to large compressive loading, such as in the housing of mechanical and power equipment, and as lateral bracing members subjected to large biaxial bending moments in orthogonal moment-resisting frames [1]. Compared with conventional universal beam and column sections, flanged cruciform sections have advantages including increased axial load-carrying capacity and savings in steel weight. These advantages arise from their increased axial resistance and geometrically symmetric configurations about both principal axes, resulting in equal section properties and flexural stiffness. Owing to these advantages, flanged cruciform section members possess great potential for use in high-rise buildings. However, despite the merits of flanged cruciform section members, their mechanical behaviour has not perhaps had the attention it deserves. Indeed, existing design codes, including the Eurocode 3 (EC3) [2] and guidance from the American Institute of Steel Construction (AISC) [3], provide no specific design recommendations for flanged cruciform section members. The present work aims to fill this gap in structural design provisions.

Flanged cruciform sections are doubly symmetric open thin-walled cross-sections and thus tend to be susceptible to torsional buckling for member lengths within certain practical ranges, as opposed to other conventional sections that are generally more susceptible to flexural buckling. Flanged cruciform sections comprise identically radiating T-shaped subsections; similar features also exist in angle sections, T-sections and plain cruciform sections, where the cross-sections comprise purely radiating outstands. For these cross-sections, the elastic torsional

* Corresponding author.
E-mail addresses: ruikai.dai20@imperial.ac.uk (R. Dai), behnam.behzadi-sofiani13@imperial.ac.uk (B. Behzadi-Sofiani), spiridione.buhagiar@um.edu.mt (S. Buhagiar), a.wadee@imperial.ac.uk (M.A. Wadee), leroy.gardner@imperial.ac.uk (L. Gardner).

https://doi.org/10.1016/j.tws.2024.112268
Received 19 April 2024; Received in revised form 28 June 2024; Accepted 22 July 2024
Available online 25 July 2024

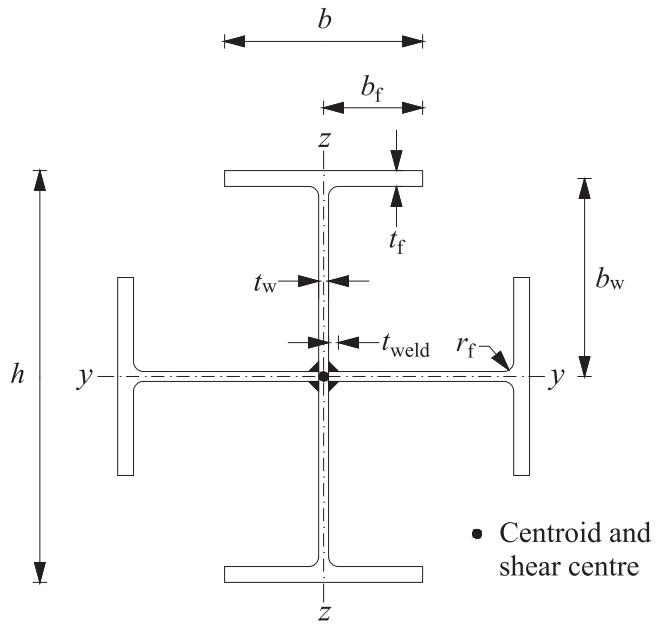

Fig. 1. Geometric configuration and adopted notation for flanged cruciform sections.

buckling load is generally more critical than the flexural counterpart, which should be considered accordingly in design specifications. However, current design provisions generally treat torsional buckling as a global buckling mode and thus instruct design engineers to adopt the global buckling curves. These curves, however, are commonly based on the theoretical and experimental results of structural members that have failed by flexural buckling. Hence, there has been an apparent mismatch within the design codes when torsional buckling is critical. Previous investigations have shown that angle section columns with similar slendernesses can exhibit very different post-buckling behaviour and ultimate resistances [4–7]. Recent works by Behzadi-Sofiani et al. on fixed-ended equal-leg angle section columns [8,9] have further revealed that the load-carrying capacity is dependent not only on the column global slenderness, but also on the ratio of the elastic torsional–flexural buckling load to the elastic minor-axis flexural buckling load. A similar finding has also been determined for plain cruciform section columns [10]. These findings suggest that the current design provisions, where the resistance reduction factor depends solely on slenderness, are not appropriate for cross-section columns that are more susceptible to torsional buckling.

The target of the present study is to develop a new resistance model for the axial load-carrying capacity of flanged cruciform section columns, which is suitable to be incorporated into future design codes. A literature review of existing theoretical and experimental works on flanged cruciform section members is presented in Section 2. The mechanical behaviour of flanged cruciform section columns is described in Section 3 with a particular emphasis on the newly developed approach for calculating the elastic local buckling load for full flanged cruciform cross-sections. A finite element (FE) model is subsequently developed using the commercial package ABAQUS [11] to simulate the mechanical behaviour of flanged cruciform section columns. The FE models are first validated against existing test results and then employed in an extended parametric study which encompasses a broader spectrum of geometric proportions for benchmark purposes. Inspired by the aforementioned recent studies [8–10], the current research reveals that the axial resistance of flanged cruciform section columns with the same torsional normalised slenderness varies with the elastic torsional to flexural buckling load ratio when torsional buckling is critical. The aforementioned shortcoming in the current EC3 provisions has therefore again been confirmed, i.e., that a single member buckling curve based on flexural buckling is not adequate for predicting the ultimate resistance of flanged cruciform section columns. The observations from the parametric study are subsequently discussed and exploited to explore the relationship between the ultimate resistance and the post-buckling stability of the associated critical buckling modes, as presented in Section 5. The test and FE results are then employed to evaluate the resistance predictions determined according to the current EC3 design provisions with the drawbacks being highlighted in Section 6. A new design approach is then proposed for predicting the ultimate resistance of flanged cruciform section columns and subsequently assessed for reliability. The proposed design approach features a new parameter that captures the variation of ultimate resistance for flanged cruciform section columns with the ratio of the elastic torsional to flexural buckling loads at the same torsional slenderness when torsional buckling is critical.

Table 1
Summary of existing experimental data on flanged cruciform section columns.

Source	Manufacturing process	No. of tests
Tahir et al. [14]	Hot-rolled & welded	4
Dobrić et al. [15]	Cold-formed & built-up	6
Total		10

2. Review of previous research

Existing research into flanged cruciform section structural components subjected to axial compression appears to be relatively scarce. Tahir and Shek [12] examined the enhancement in load-carrying capacity of flanged cruciform section columns over their bare I-section counterparts based on the design provisions of BS 5950-1 [13], and highlighted the advantages of the former, including increased axial stiffness and resistance. Tahir et al. [14] subsequently conducted experiments on flanged cruciform section columns alongside their universal beam section counterparts; torsional failure was observed for the tested members with intermediate slenderness levels, while local failure within the flanges was deemed dominant for the more stocky tested members. Dobrić et al. [15] conducted experiments on cold-formed stainless steel built-up flanged cruciform section columns, where the specimens comprised six plain channel section columns bolted together at intervals with two different patterns; short, intermediate and long member lengths were tested. It was observed that the buckling patterns were affected by both the global slenderness of the members and by the spacing between the fasteners; for the short columns, failure was dominated by local buckling and thus the spacing between fasteners was a governing factor, while for the longer columns, where torsional buckling was critical, the influence of the spacing of fasteners became minimal. A summary of the existing experimental data reported on flanged cruciform section columns is presented in Table 1.

Studies have also been conducted on flanged cruciform section components under other loading scenarios. Harris and Urgessa [1] examined the strength of flanged and plain cruciform section members subjected to combined compression and bending. It was reported that the flexural performance of flanged cruciform section members was superior to their plain cruciform counterparts at all slenderness levels; moreover, flanged cruciform section members were deemed suitable for engineering applications involving high levels of compression and biaxial bending. Kiani et al. [16] focused on the local seismic stability of flanged cruciform section beam–column members subjected to axial compression combined with cyclic uniaxial bending; a new residual stress distribution pattern alongside an appropriate geometric imperfection pattern were proposed and subsequently employed in numerical models. Similar studies were conducted for the panel zone design detailing of flanged cruciform section members in seismic applications [17–19]. Svensson and Plum [20] proposed a

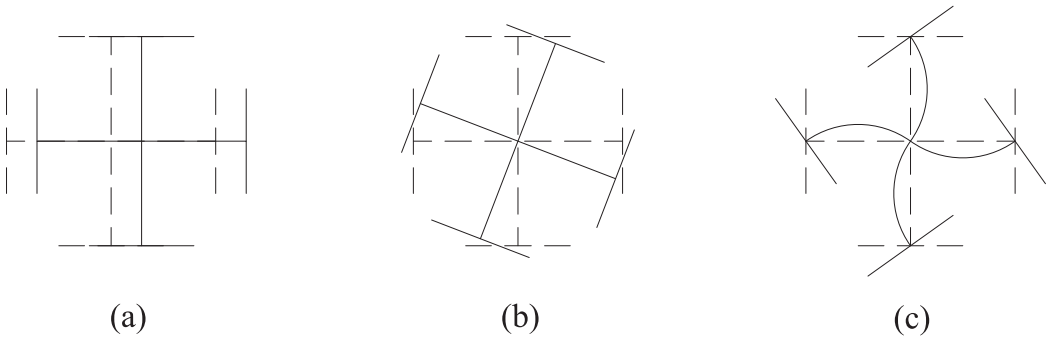

Fig. 2. Distinct elastic (a) flexural, (b) torsional and (c) local cross-section buckling displacement patterns for flanged cruciform section columns subjected to axial compression.

means of increasing the torsional buckling strength of flanged cruciform members by adopting intermediate stiffener plates welded between adjacent flanges. Similar suggestions on improving web stiffness through intermediate gusset plates have also been made by King [21].

3. Mechanical behaviour

The buckling behaviour of a flanged cruciform section member subjected to uniform axial compression can be categorised into global (flexural and torsional) and local displacement patterns, as illustrated in Fig. 2. The flexural displacement pattern, which typically dominates for long members, is characterised by the translational displacement of the cross-section centroid. The torsional displacement pattern is characterised by rigid-body twist of the whole cross-section about its shear centre, which coincides with the centroid for flanged cruciform sections. This torsional buckling pattern is predominant in flanged cruciform section columns of short-to-medium length. The local displacement pattern is characterised by instability of the constituent plates of a flanged cruciform section; this pattern is generally observed in very short flanged cruciform section columns. Similar buckling behaviour has also been found in previous studies into fixed-ended equal-leg angle section columns and plain cruciform section columns [8,10].

The formula for calculating the elastic flexural buckling load of flanged cruciform section columns is given from the standard Euler buckling load thus:

$$N_{\mathrm{cr,F}} = \frac{\pi^2 EI}{L^2_{\mathrm{cr,F}}} \tag{1}$$

where E is the Young's modulus of the material, I is the second moment of area of the cross-section about the appropriate axis, and $L_{\mathrm{cr,\ F}}$ is the effective flexural buckling length.

The formula for calculating the elastic torsional buckling load of flanged cruciform section columns is provided in [22] as:

$$N_{\mathrm{cr,T}} = \frac{1}{i_0^2}\left[GJ + \frac{\pi^2 EI_{\mathrm{w}}}{L^2_{\mathrm{cr,T}}}\right] \tag{2}$$

where i_0 is the polar radius of gyration of the cross-section with respect to its shear centre, G is the shear modulus of the material, J is the St. Venant torsion constant, I_{w} is the warping stiffness and $L_{\mathrm{cr,T}}$ is the effective torsional buckling length about the longitudinal axis, which is the distance between adjacent inflexion points of the twisted shape [23]. In this formula the stress in the through-thickness direction is assumed to be zero and the effect of Poisson's ratio ν is neglected. If the latter effect were considered by assuming that anticlastic plate bending is restrained due to plate continuity, the familiar $(1-\nu^2)$ term appears in the denominator of the warping associated term [8,10]:

$$N_{\mathrm{cr,T}} = \frac{1}{i_0^2}\left[GJ + \frac{\pi^2 EI_{\mathrm{w}}}{L^2_{\mathrm{cr,T}}(1-\nu^2)}\right] \tag{3}$$

where $G = E/[2(1+\nu)]$ for isotropic materials, $L_{\mathrm{cr,T}} = L/2$ when both ends of the member are fixed against rotation and warping, while i_0, J and I_{w} for a flanged cruciform section can be calculated respectively, thus:

$$i_0^2 = i_{\mathrm{p}}^2 + y_0^2 + z_0^2, \quad i_{\mathrm{p}}^2 = \frac{I_{\mathrm{y}} + I_{\mathrm{z}}}{A}, \tag{4}$$

$$J = \frac{4}{3}b_{\mathrm{w}}t_{\mathrm{w}}^3 + \frac{8}{3}b_{\mathrm{f}}t_{\mathrm{f}}^3, \quad I_{\mathrm{w}} = \frac{8b_{\mathrm{w}}^2 b_{\mathrm{f}}^3 t_{\mathrm{f}}}{3}. \tag{5}$$

Here, I_{y} and I_{z} are the second moments of area of the cross-section about its principal axes, A is the cross-sectional area and y_0 and z_0 are the distances between the shear centre and centroid in the y and z directions, respectively, which are both equal to zero for a doubly-symmetric flanged cruciform section; b_{w} and t_{w} are the width and thickness of the web, respectively, while b_{f} and t_{f} are the width and thickness of the flange, respectively, as shown in Fig. 1.

The formula for calculating the elastic local buckling load of flanged cruciform section columns is defined thus:

$$N_{\mathrm{cr,L}} = A\sigma_{\mathrm{cr,cs}} \tag{6}$$

where $\sigma_{\mathrm{cr,cs}}$ is the local buckling stress of the full flanged cruciform section. This full cross-sectional local buckling stress is determined by accounting for the interaction between individual constituent plate elements. This element interaction is embodied through an interaction coefficient ζ that ranges between 0 and 1, and is bound by the theoretical limits of the local buckling stress of the isolated critical plates with simply supported and fixed boundary conditions along the adjoined edges [24,25]. The general formula for determining the elastic local buckling stress of the full cross-section $\sigma_{\mathrm{cr,cs}}$ is given thus:

$$\sigma_{\mathrm{cr,cs}} = \sigma^{\mathrm{SS}}_{\mathrm{cr,p}} + \zeta\left(\sigma^{\mathrm{F}}_{\mathrm{cr,p}} - \sigma^{\mathrm{SS}}_{\mathrm{cr,p}}\right) \quad \text{where} \quad 0 \le \zeta \le 1 \tag{7}$$

where $\sigma^{\mathrm{SS}}_{\mathrm{cr,p}}$ is the local buckling stress of the isolated critical plate with simply supported boundary conditions and $\sigma^{\mathrm{F}}_{\mathrm{cr,p}}$ is the local buckling stress of the isolated critical plates with fixed boundary conditions along the adjoined edges.

Functions for determining the interaction coefficient for a series of common cross-section shapes are provided in [24]. The functions for determining the interaction coefficient ζ for flanged cruciform sections under uniform axial compression are developed herein based on the results of finite strip analyses, where the full cross-section elastic local buckling stresses $\sigma_{\mathrm{cr,cs}}$ for a comprehensive range of geometries have been determined. The interaction coefficient ζ can be back-calculated by rearranging Eq. (7) thus:

$$\zeta = \frac{\sigma_{\mathrm{cr,cs}} - \sigma^{\mathrm{SS}}_{\mathrm{cr,p}}}{\sigma^{\mathrm{F}}_{\mathrm{cr,p}} - \sigma^{\mathrm{SS}}_{\mathrm{cr,p}}} \quad \text{where} \quad 0 \le \zeta \le 1. \tag{8}$$

The elastic local buckling stresses of 2482 flanged cruciform sections under uniform axial compression were obtained through finite strip analysis (FSA) using the software CUFSM v5.04 [26,27]. Within the analyses, the individual constituent plates of the cross-section were discretised into 8 strips along their centreline geometry. The centreline approximation is slightly conservative since the small beneficial

Table 2
Plate buckling coefficients k with different boundary conditions.

Scenario	Boundary conditions*		Formulae for plate buckling coefficient k	k value for long plates
	Unloaded edge 1	Unloaded edge 2		
$\sigma^{F}_{cr,w}$	F	SS	$k = \frac{76(1-\nu)}{\pi^2} + \frac{0.6}{(a_{eff}/b)^2}$	5.42
$\sigma^{SS}_{cr,w}$	SS	SS	$k = \frac{56(1-\nu)}{\pi^2} + \frac{0.7}{(a_{eff}/b)^2}$	4.00
$\sigma^{F}_{cr,f}$	F	Fr	$k = \frac{18(1-\nu)}{\pi^2} + \frac{0.7}{(a_{eff}/b)^2}$	1.25
$\sigma^{SS}_{cr,f}$	SS	Fr	$k = \frac{6(1-\nu)}{\pi^2} + \frac{1}{(a_{eff}/b)^2}$	0.43

* 'SS' – simply supported, 'F' – fixed, 'Fr' – free.

effects provided by the fillets, which reduces the plate flat width and provides additional restraints, are ignored [24]. A Young's modulus $E = 210,000$ MPa and a Poisson's ratio $\nu = 0.3$ were adopted throughout the analyses. The normalised cross-section dimensions, defined as $(b_w/t_w) \cdot (t_f/b_f)$ in accordance with [24], range between 0.8 and 20 in this parametric study; this range encompasses the cross-sections used in engineering practice. The auxiliary parameter ϕ is introduced thus:

$$\phi = \frac{\sigma^{SS}_{cr,f}}{\sigma^{SS}_{cr,w}} \tag{9}$$

which defines the relative susceptibility of the flange and the web to local buckling at the simply supported lower bound [24]. Note that Eq. (9) is a simplified equation and only applies to cases where the maximum applied compressive stresses for the flange and the web are identical (i.e., $\sigma_{max,f} = \sigma_{max,w}$, which is the case throughout the present paper since the studied members are under uniform compression). The well-known formula for calculating the elastic buckling stress $\sigma_{cr,p}$ of a rectangular plate of width b and thickness t, is given thus:

$$\sigma_{cr,p} = k\frac{\pi^2 E}{12(1-\nu^2)}\left(\frac{t}{b}\right)^2 \tag{10}$$

where k is the plate buckling coefficient for a uniaxially loaded plate, which depends on the boundary conditions on its loaded and unloaded edges, and the plate aspect ratio a/b, where a is the plate length and b is the plate width. The plate buckling coefficients k were established through numerical modelling in ABAQUS [11], where the plate width-to-thickness ratio b/t ranges between 50 and 100 and the plate aspect ratio a/b ranges between 0.5 and 10. Note that the boundary conditions on the loaded edges of the plates were fixed in the FE models; hence, the effective plate aspect ratio a_{eff}/b is adopted in the formulae, where $a_{eff} = a/2$ is the effective length of the plate, with a being the full length of the plate. Based on the numerical results, length dependent predictive formulae for k were developed. The formulae, alongside the values for long plates, which accorded with those reported in the literature [22,28–30], are listed in Table 2.

The critical isolated plate (i.e., flange or web) is defined as the one with the minimum elastic critical buckling stress. Hence,

$$\sigma^{SS}_{cr,p} = \min(\sigma^{SS}_{cr,w},\ \sigma^{SS}_{cr,f}), \tag{11}$$

$$\sigma^{F}_{cr,p} = \min(\sigma^{F}_{cr,w},\ \sigma^{F}_{cr,f}). \tag{12}$$

The back-calculated interaction coefficient ζ versus ϕ is obtained for flanged cruciform sections under uniform axial compression. Note that the lowest interaction coefficient ζ actually occurs where $\phi \approx 0.45$. The minimum ζ is expected to occur at $\phi = 1$, where the critical buckling stresses of the flange and the web are identical. The difference with the expected minimum at $\phi = 1$ is explained by the fact that there is a region between approximately $0.45 \le \phi \le 1$ where the upper bound limit for the cross-section local buckling stress is defined by the web, while the lower bound is defined by the flange. Therefore, since the interaction coefficient ζ also depends on the upper bound limit, which tends to increase at a higher rate than the full cross-section local buckling stress in this transition region, the minimum of ζ is shifted to the point where the local buckling stresses of the isolated flange and web with fixed boundary conditions are approximately equal (i.e., $\sigma^{F}_{cr,f} \approx \sigma^{F}_{cr,w}$). Similar phenomena can also be observed for I-sections subjected to combined compression and major axis bending [24].

Table 3
Proposed formulae for the interaction coefficient ζ for flanged cruciform sections subjected to axial compression.

Load case	Flange critical ($\phi < 1$)	Web critical ($\phi \ge 1$)
Compression	$\zeta = \frac{t_w}{t_f}(0.525 - 0.5\phi) \ge \frac{t_f}{t_w}(0.01 + 0.3\phi)$	$\zeta = \frac{t_f}{t_w}(0.41 - 0.1\phi^{-3})$

Table 4
Statistical assessment of elastic local buckling stress predictions using proposed formulae and the isolated plate assumption (EC3) versus the numerical (CUFSM) results for flanged cruciform sections subjected to axial compression.

Proposed/CUFSM		EC3/CUFSM	
Mean	CoV	Mean	CoV
0.983	0.023	0.780	0.090

The proposed formulae for the interaction coefficient ζ for flanged cruciform sections subject to axial compression are shown in Figs. 3(b) and 4(b) alongside Table 3. Note that the interaction coefficient ζ is considered to be dependent on both the cross-sectional geometry and the member length through the auxiliary parameter ϕ, which is a function of the elastic buckling stresses of the most critical flange and web elements, as shown in Eq. (9); these stresses, as shown in Eq. (10), are functions of the cross-sectional geometry through t and b, and of the member length through k, respectively.

The full cross-section elastic local buckling stresses determined based on the proposed formulae are compared against the FSA results and the elastic buckling stress of the isolated critical plate from within the cross-section in Fig. 5 in the form of normalised frequency distributions. The numerical comparisons are presented in Table 4, which demonstrate that the proposed formulae provide significantly better predictions than the current EC3 approach which only considers isolated plate elements within the cross-section. The mean full cross-section local buckling stress prediction is 0.983 of the FSA results with a CoV of 0.023, which is accurate and slightly safe sided, compared to a mean prediction of 0.780 with a CoV of 0.090 when the element interaction within the cross-section is neglected.

The variation of the elastic buckling load N_{cr} with respect to the member length L (on a logarithmic scale) for a typical flanged cruciform section column FC $100 \times 50 \times 5 \times 5$ (flanged cruciform web width $b_w \times$ flange width $b_f \times$ web thickness $t_w \times$ flange thickness t_f in mm) is shown in Fig. 6. It may be observed that local buckling is critical for short-length flanged cruciform section columns, whereas for intermediate lengths the critical buckling mode transitions from local to torsional buckling; then flexural buckling dominates for longer lengths. Note that the proposed formulae for determining the elastic local buckling load for flanged cruciform section columns agree well with the numerical data points.

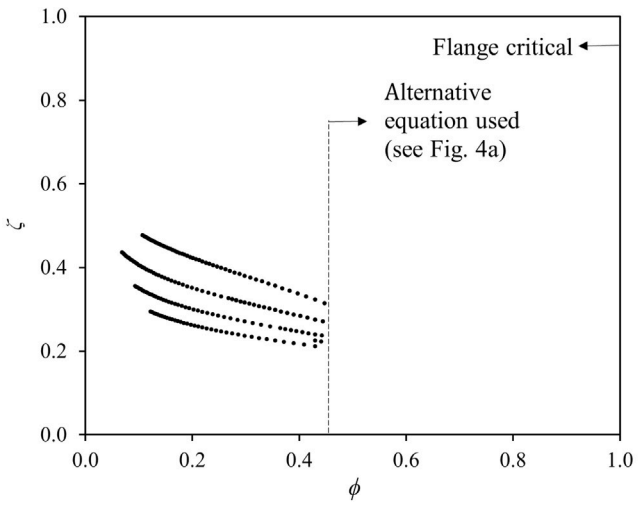

(a) Back calculated ζ versus ϕ

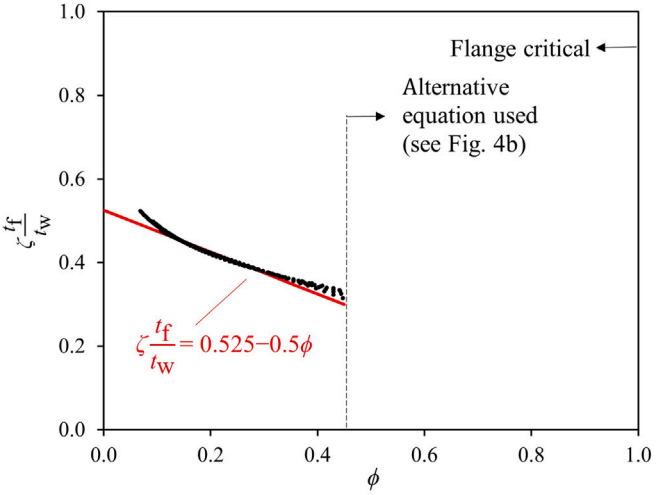

(b) Back calculated $\zeta\frac{t_f}{t_w}$ versus ϕ

Fig. 3. Developed ζ functions for flanged cruciform sections with $\phi \lesssim 0.45$ subjected to uniform axial compression: (a) scatter of the back calculated interaction coefficient ζ and (b) reduced scatter and proposed functions incorporating the geometric factor t_f/t_w.

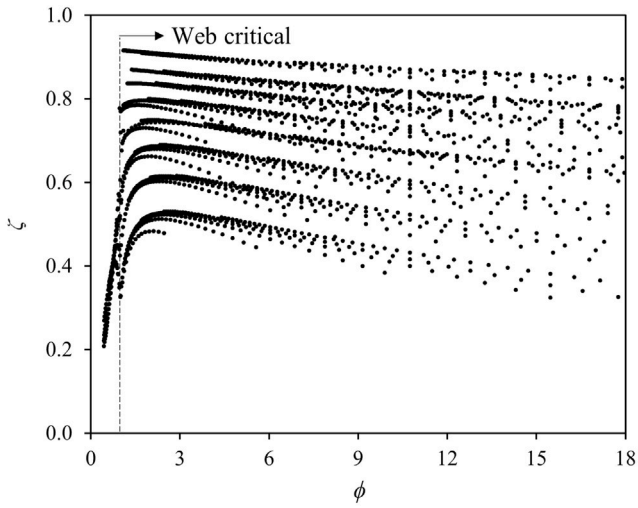

(a) Back calculated ζ versus ϕ

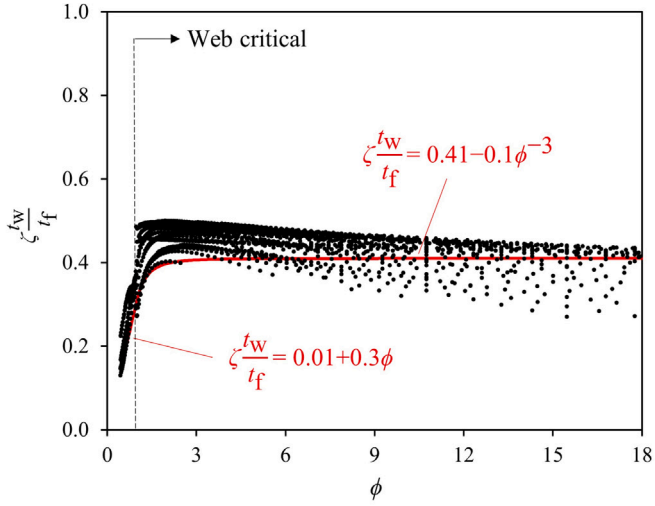

(b) Back calculated $\zeta\frac{t_w}{t_f}$ versus ϕ

Fig. 4. Developed ζ functions for flanged cruciform sections with $\phi \gtrsim 0.45$ subjected to uniform axial compression: (a) scatter of the back calculated interaction coefficient ζ and (b) reduced scatter and proposed functions incorporating the geometric factor t_w/t_f.

4. Numerical modelling

Finite element (FE) modelling with the commercial package ABAQUS [11] has been conducted to simulate the mechanical behaviour of flanged cruciform section columns subject to axial compression. The principal features of the numerical models, including material properties, residual stress patterns, geometric imperfections and boundary conditions, are described in this section. Validation of the FE models against existing experimental results is presented. The validated FE models are subsequently employed to conduct a comprehensive parametric study to investigate the mechanical behaviour of flanged cruciform section columns with a broad spectrum of geometric proportions.

4.1. General modelling assumptions

The 4-noded shell element, with reduced integration, hourglass control and 6 degrees of freedom (3 translational and 3 rotational) at each node has been employed to model the flanged cruciform section members. This element, referred to as 'S4R' in the ABAQUS element library [11], is suitable for the simulation of both thin-walled and thick-walled cross-sections and has been successfully employed in previous studies for similar applications [8,10,31–34]. A mesh size of approximately 5 mm was employed throughout the numerical modelling process, which typically resulted in at least 10 elements along each web and flange of the flanged cruciform cross-sections. This mesh size was determined through a mesh sensitivity analysis and showed a good balance between accuracy of results and computational expense.

For the root fillets of the two constituent hot-rolled I-sections and the fillet welds at the central web intersection, thicker elements were introduced at these junctions, as shown in Fig. 7. The nodes at these junctions were connected using 'BEAM' type multi-point constraints (MPC). The number of elements, alongside their widths and thicknesses were determined such that the targeted geometric features were captured accurately while maintaining reasonably low aspect ratios for these elements.

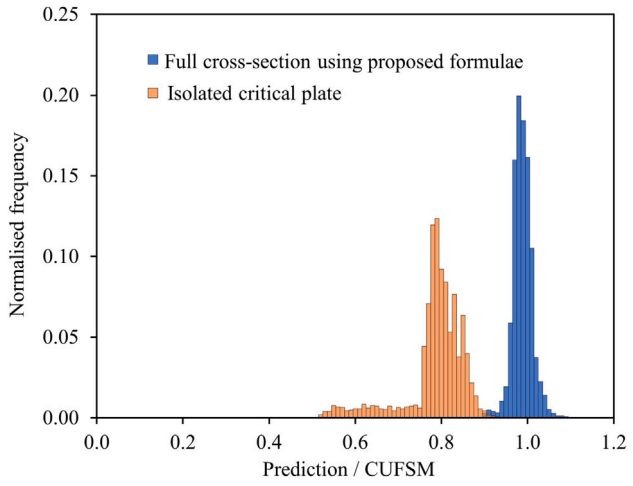

Fig. 5. Normalised frequency distributions for predicted full cross-section and isolated plate elastic buckling stresses versus FSA results obtained from CUFSM for flanged cruciform sections subjected to axial compression.

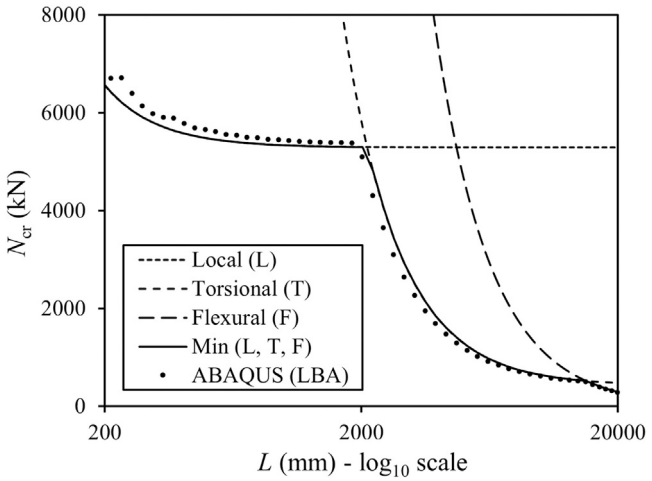

Fig. 6. Elastic buckling load N_{cr} for different buckling modes plotted against member length L for a flanged cruciform section (FC $100\times50\times5\times5$) column with fixed-ended boundary conditions.

The nodes at each end of the member were linked to reference points through kinematic coupling restraints, which allowed a uniform load distribution and formed warping-fixed boundary conditions. The boundary conditions against torsion and flexure were then imposed on these two reference points by restraining their corresponding rotational and translational degrees of freedom. A longitudinal displacement was applied to the top reference point to model the axial compressive load. The geometrically and materially nonlinear analyses with imperfections (GMNIA) were conducted using the Riks arc-length method [35].

4.2. Material modelling

For validation purposes, all existing, as far as the authors are aware, reported experiments on flanged cruciform section columns subject to axial compression were simulated. The measured material stress–strain curves, where available, were adopted in the numerical simulations; where not available, and throughout the parametric study, the material models developed by Yun and Gardner [36] for hot-rolled steels and by Gardner and Yun [37] for cold-formed steels were adopted. The hot-rolled steel material model [36] is a two-stage piecewise linear plus nonlinear hardening model featuring an elastic response up to the yield point, followed by a yield plateau and strain hardening up to the ultimate tensile stress. The cold-formed steel material model [37] is a two-stage Ramberg–Osgood model with standardised values for the strain-hardening exponents, featuring a rounded stress–strain response with no sharply defined yield point. A Poisson's ratio of 0.3 in the elastic range was assumed in all cases. The material properties were input into ABAQUS in the form of true stress σ_{true} and true plastic strain ϵ_{true}, which were converted from the measured engineering stress σ and strain ϵ values using the following standard equations:

$$\sigma_{true} = \sigma(1+\epsilon), \quad \epsilon_{true} = \ln(1+\epsilon) - \frac{\sigma_{true}}{E}. \tag{13}$$

4.3. Residual stresses

Residual stresses are generated inevitably throughout the manufacturing process, in particular from differential cooling in hot-rolled and welded structural elements. The presence of these residual stresses tends to cause the earlier onset of material yielding and consequently a reduction in ultimate resistance; hence they need to be incorporated in numerical models. To the best of the authors' knowledge, there is no existing experimental study into the residual stresses distribution of flanged cruciform sections. However, Kiani et al. [16] proposed a rational residual stress pattern for flanged cruciform sections based on I-sections and welded plain cruciform sections that is currently adopted. The magnitude and distribution of the residual stresses in the flanges and at the web–flange junctions were considered to be similar to those of I-sections [38], while those at the central web intersection were based on a proposed model for welded plain cruciform sections [39]. This residual stress pattern, as shown in Fig. 8, was employed for validation, where reported residual stresses were not available, and throughout the parametric study. Note that Fig. 8 demonstrates the residual stress pattern for a typical flange and web; the remaining flanges and webs have identical residual stress distributions. The residual stresses were input into ABAQUS using the *INITIAL CONDITIONS command [40].

4.4. Initial geometric imperfections

Initial geometric imperfections for flanged cruciform section members can include one or a combination of the following patterns: a global member out-of-straightness, a cross-section twist, and a deviation from flatness of the individual constituent plate elements. These initial geometric imperfections can significantly influence the mechanical response and ultimate capacity of the structural members and thus should be incorporated into the numerical models. Initial geometric imperfections, which arise during the manufacturing, handling and erection processes, are inherent to the structural elements and can essentially assume any form within the bounds of the manufacturing tolerances. Note that both the shape and amplitude of the initial geometric imperfections affect the ultimate resistances of members in FE simulations. Therefore, for validation purposes, the measured initial geometric imperfections reported in the literature, where possible, were adopted in the numerical models. In cases where measured initial geometric imperfections were not available, and throughout the parametric study, a combination of all the three aforementioned imperfections were employed, as considered in previous studies on similar cross-sections [8–10] and recommended in design provisions [41]. Generally, the following imperfections were introduced into the FE models, as shown in Fig. 9: (1) a half sinusoidal wave bow-shaped imperfection over the full member length with an amplitude of $L/1000$ at midspan about both principal axes, (2) a similar shape for the initial twist with an amplitude of $\theta = \arctan[L/(1000b_w)]$ at midspan and (3) a periodic double sinusoidal wave with an amplitude of $b_w/250$ in the webs (a half sinusoidal wave across the web width b_w in conjunction with a periodic sinusoidal wave with a half-wavelength of $L_{b,cs}$ along the member length), and a similar periodic sinusoidal wave in the

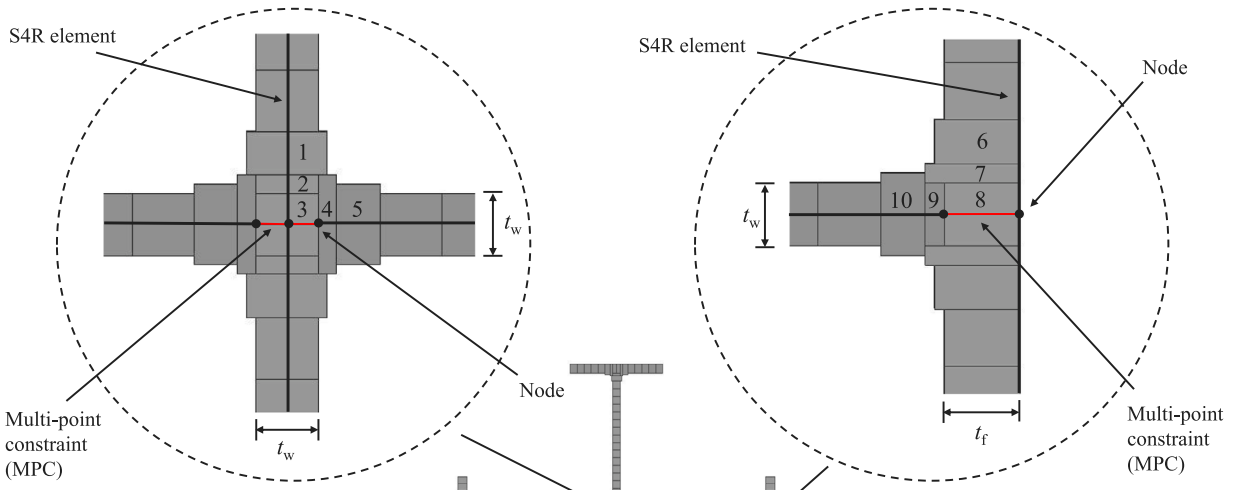

Element number	Width	Thickness
1	$0.7t_w$	$1.3t_w$
2	$0.3t_w$	t_w
3	$0.5t_w$	t_w
4	$0.3t_w$	$1.6t_w$
5	$0.7t_w$	$1.3t_w$

Element number	Width	Thickness
6	$0.7t_w$	$t_f + 0.15t_w$
7	$0.3t_w$	$t_f + 0.3t_w$
8	$0.5t_w$	t_f
9	$0.3t_w$	t_w
10	$0.7t_w$	$1.3t_w$

Fig. 7. Representation of junction regions for flanged cruciform sections in the FE models.

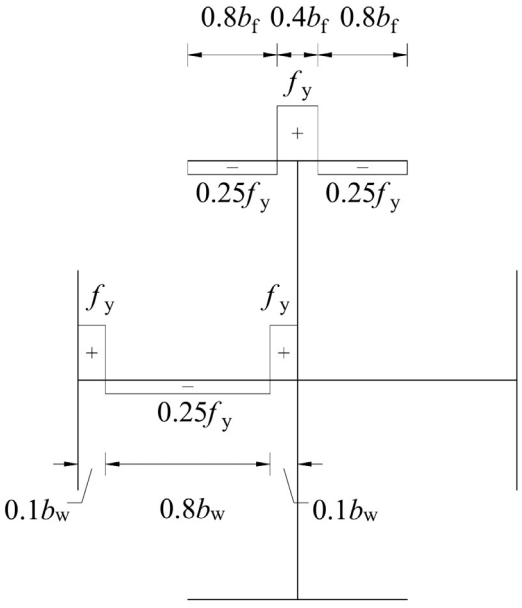

Fig. 8. Residual stress pattern for flanged cruciform sections in the FE models.

flanges to maintain orthogonality between adjacent webs and flanges. The local buckling half-wavelength $L_{b,cs}$ of the whole flanged cruciform cross-section was determined through the interaction coefficient ζ developed in Section 3 following similar procedures for I-sections specified in [42].

4.5. Validation

The FE models were validated against a total of 10 tests on flanged cruciform section columns, where 4 specimens were fabricated by welding two hot-rolled universal beam sections [14], and 6 specimens were built-up using six cold-formed plain channel sections [15]. In the absence of measured imperfection and residual stresses in [14], a slightly enlarged initial geometric imperfection was employed in the FE models to account for possible unfavourable factors including eccentric loading and additional welding induced out-of-straightness. For validation purposes against [15], the FE model was modified to feature the influence of bolting and the measured material properties. A summary of comparisons between the numerical and experimental results of ultimate loads is presented in Table 5 and Fig. 10. The FE results show good agreement with the experimental results with a mean $N_{u,FE}/N_{u,Test}$ ratio of 1.00, where $N_{u,FE}$ and $N_{u,Test}$ are the ultimate loads from the FE simulations and tests, respectively, and a coefficient of variation (CoV) of 0.04. A typical load versus average axial strain comparison between the FE results and the experimental data reported in [14] is presented in Fig. 11. Given that the measured geometric imperfections and residual stresses were not reported, the FE and test results are deemed to show good agreement. The numerical models are thus considered to be suitably validated for use within further parametric analyses.

Table 5
Comparison between numerical and experimental results of ultimate loads $N_{u,FE}/N_{u,Test}$.

Source	Manufacturing process	No. of tests	$N_{u,FE}/N_{u,Test}$			
			Mean	CoV	Min	Max
Tahir et al. [14]	Hot-rolled & welded	4	1.01	0.04	0.96	1.06
Dobrić et al. [15]	Cold-formed & built-up	6	0.99	0.04	0.93	1.04
Total		10	1.00	0.04	0.93	1.06

4.6. Parametric study

Following the validation of the FE models, a parametric study is presented that explores the mechanical behaviour of spherically-pinned flanged cruciform section columns with a broad spectrum of cross-sectional geometric proportions and member lengths. The material stress–strain response for hot-rolled steel proposed by Yun and

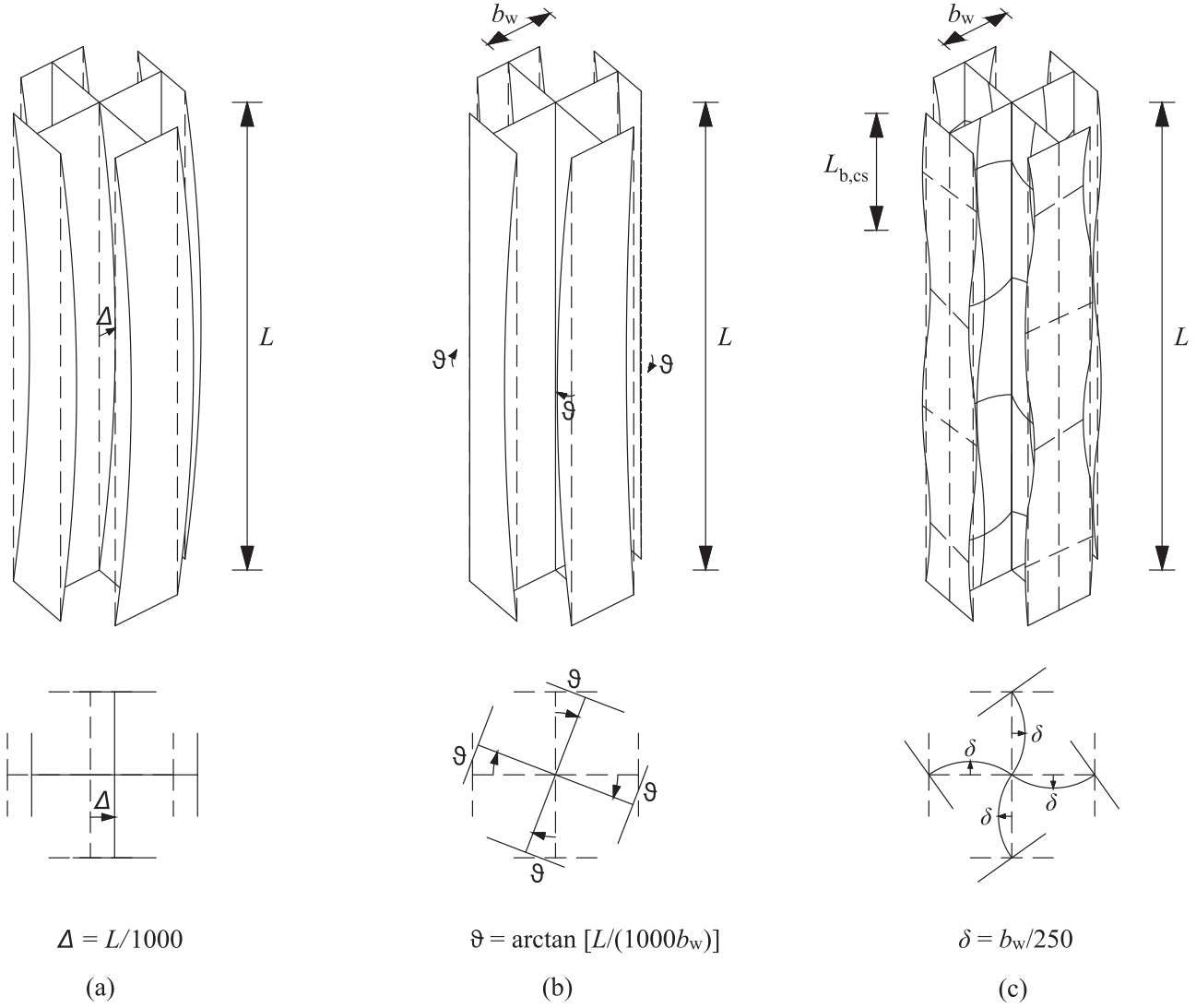

Fig. 9. Initial geometric imperfection shapes: (a) flexural, (b) torsional and (c) local, with amplitudes employed in the FE parametric studies.

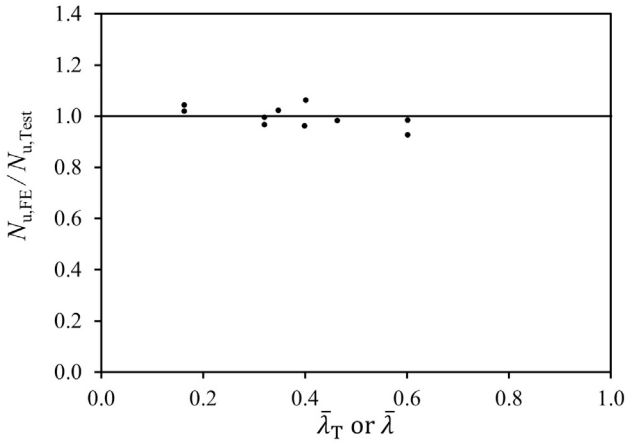

Fig. 10. Comparison between numerical and experimental results of ultimate loads $N_{u,FE}/N_{u,Test}$ against the higher normalised slenderness $\bar{\lambda}_T$ or $\bar{\lambda}$ (i.e., more critical).

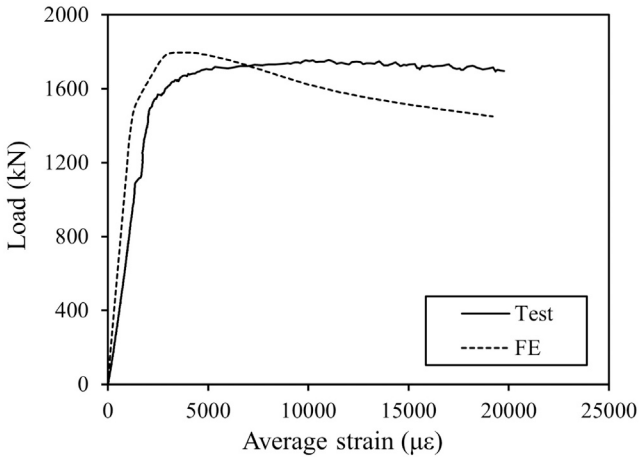

Fig. 11. Typical load versus average strain relationship from FE and experimental results reported in [14].

Gardner [36] was employed throughout the parametric study. Steel grade S355 with a yield stress f_y = 355 N/mm^2, an ultimate stress f_u = 490 N/mm^2 and a Young's Modulus E = 210,000 N/mm^2 were adopted, in accordance with EN 1993-1-1 [2,43]. The width of the web

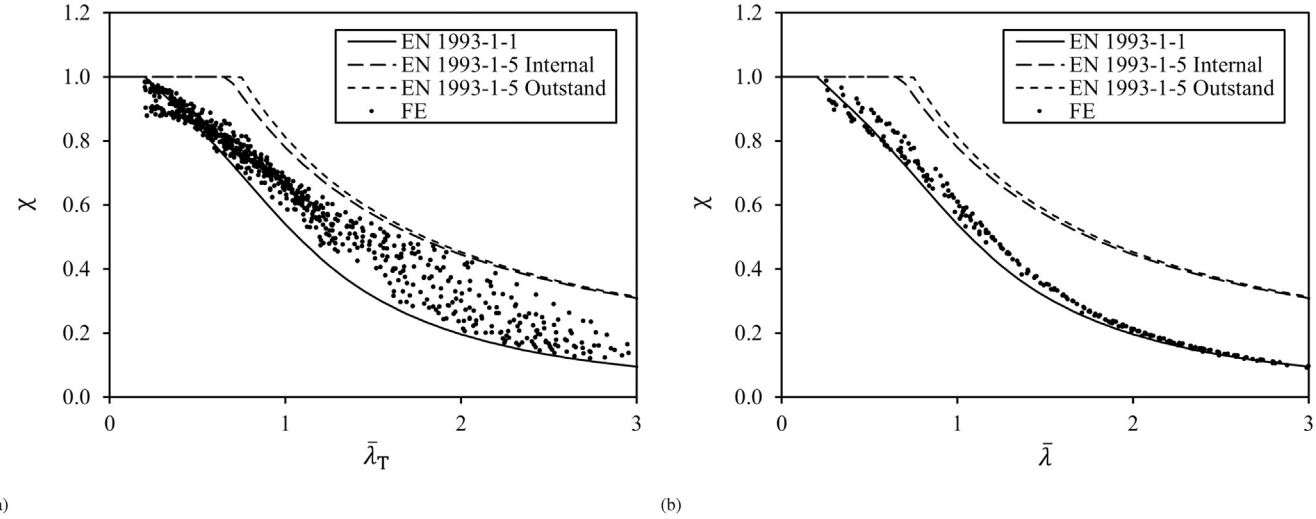

Fig. 12. Comparison of FE results for spherically-pinned steel flanged cruciform section columns against EC3 buckling curves where: (a) torsional buckling is critical (i.e., $N_{cr,T} \leq N_{cr,F}$) with $\bar{\lambda}_T = \sqrt{Af_y/N_{cr,T}}$ where $A = A_{eff}$ for Class 4 sections, and (b) flexural buckling is critical (i.e., $N_{cr,F} < N_{cr,T}$) with $\bar{\lambda} = \sqrt{Af_y/N_{cr,F}}$ where $A = A_{eff}$ for Class 4 sections.

b_w was fixed at 100 mm, while all other geometric parameters, i.e., the flange width b_f, web thickness t_w, flange thickness t_f and member length L, were varied to generate a broad spectrum of geometric proportions, normalised slenderness, $\bar{\lambda}_T$ or $\bar{\lambda}$, and elastic buckling load ratios $N_{cr,T}/N_{cr,F}$. The b_w/b_f ratios ranged between 1.5 and 5; the b_w/t_w ratios ranged between 20 and 40; the t_f/t_w ratios ranged between 1.2 and 2; the L/b_w ratios ranged between 5 and 120. In total, 1115 FE results were produced, which are presented in terms of the reduction factor χ plotted against the corresponding normalised slenderness in Fig. 12. For reference purposes, the plate buckling curves for internal and outstand elements from EN 1993-1-5 [41] and the flexural buckling curve with limiting normalised slenderness $\bar{\lambda}_0 = 0.2$ and imperfection factor $\alpha = 0.49$ from EN 1993-1-1 [2] are superimposed on the graphs in Fig. 12. According to the current design approach specified in EN 1993-1-1 [2], flanged cruciform section column members with the same normalised slenderness should have the same member reduction factors. However, it is shown in Fig. 12 that for cases where torsional buckling is critical (i.e., $N_{cr,T} \leq N_{cr,F}$), flanged cruciform section columns with the same normalised member slenderness could have highly varying member buckling reduction factors; this phenomenon is particularly prominent for more slender members. This vertical spread of data points at the same member slenderness is closely related to the varying elastic buckling load ratio $N_{cr,T}/N_{cr,F}$ and the correspondingly different post-buckling behaviour. As shown in Fig. 12(a), when $N_{cr,T}/N_{cr,F}$ is low, torsional buckling dominates and the corresponding data points lie closer to the plate buckling curves from EN 1993-1-5 [41]; as the ratio approaches unity and flexural buckling begins to interact with torsional buckling, the buckling reduction factor decreases and converges to the flexural buckling curve from EN 1993-1-1 [2]. When the ratio surpasses unity, flexural buckling becomes dominant and the data points generally follow the column buckling curve, as shown in Fig. 12(b).

5. Analysis and discussion of results

Following the examination of the numerical results, a further in-depth investigation was conducted to understand the mechanical behaviour behind the observed phenomena. The torsional post-buckling behaviour of flanged cruciform section columns was investigated analytically first. In previous cases, such as equal-leg angle section columns [4–8,44] and plain cruciform section columns [10], where torsional and local buckling have been shown to be essentially identical modes, the stable torsional post-buckling behaviour was attributed to the membrane stretching of the plates. However, this explanation does not hold for flanged cruciform section columns since torsional and local buckling modes are no longer identical. Existing literature has presented analytical investigations of the flexural–torsional buckling and post-buckling behaviour of thin-walled open sections [45–48]. Therein, large deflections were considered through Green's strain tensor [46,47], and the shortening effect was considered in the torsion equilibrium equation [47]. These considerations, as opposed to the classic linear analysis in [22,23], incorporated higher order terms into the general differential equation for torsional buckling, thus:

$$EI_w \frac{d^4\theta}{dx^4} + \left(N\frac{I_0}{A} - GJ\right)\frac{d^2\theta}{dx^2} - \frac{3}{2}EI_{ht}\left(\frac{d\theta}{dx}\right)^2\frac{d^2\theta}{dx^2} = 0 \tag{14}$$

where x is along the longitudinal direction of the member, θ is the angle of twist of the cross-section about the x-x axis and N is the axial compressive load; E and G are the Young's and shear modulus of the material, respectively; J and I_w are the St. Venant torsion constant and warping constant, respectively, as previously defined in Eq. (5); $I_0 = I_y + I_z$, which is the polar second moment of area, as previously defined in Eq. (4); I_{ht} is the higher order torsion constant given thus:

$$I_{ht} = I_R - \frac{I_0^2}{A} \tag{15}$$

where I_R is the polar fourth moment of area defined as:

$$I_R = \int_A \left[(y-y_0)^2 + (z-z_0)^2\right]^2 dA \tag{16}$$

with y_0 and z_0 being shear centre coordinates that are both equal to zero for a doubly-symmetric flanged cruciform section. Approximate solutions of Eq. (14) can be obtained using Galerkin's method [47] assuming a trigonometric function $\theta_0 = \theta \sin(\pi x/L)$, where θ_0 is the maximum angle of twist of the cross-section at the midspan of the member. This may be further simplified to predict the pre- and post-buckling behaviour for a doubly-symmetric flanged cruciform section analytically and leads to the following equations:

$$\begin{aligned} \theta_0 &= 0 \\ N - N_{cr,T} &= \frac{3\pi^2 EAI_{ht}}{8L^2 I_0}\theta_0^2. \end{aligned} \tag{17}$$

This solution presented in Eq. (17) indicates a stable and symmetric post-buckling behaviour for flanged cruciform section columns. Geometrically nonlinear analyses with imperfections (GNIA) were also

conducted currently within ABAQUS, where the geometric imperfections were set to very small magnitudes, i.e., 1/100 of the values employed in the parametric study, such that the corresponding buckling modes could be triggered with the post-buckling path not deviating significantly from that of the geometrically perfect members. The relationship between the axial load N normalised by the elastic buckling load N_{cr} and (a) the axial shortening δ normalised by the axial shortening at the elastic buckling load δ_{cr}, and (b) the angle θ_0 (for torsional buckling critical cases, i.e., $N_{cr,T} \leq N_{cr,F}$), are presented in Figs. 13(a) and 13(b) respectively for flanged cruciform section columns with five $N_{cr,T}/N_{cr,F}$ values between 0.4 and 1.2 and the same member slenderness $\bar{\lambda}_T$ or $\bar{\lambda}$. It is observed in Fig. 13(b) that for cases where torsional buckling is critical (i.e., $N_{cr,T} \leq N_{cr,F}$), the initial post-buckling paths are all stable; when the elastic buckling load ratio $N_{cr,T}/N_{cr,F}$ increases and nears unity, the onset of the transition from stable torsional post-buckling behaviour to almost neutral flexural post-buckling behaviour occurs earlier; for cases where flexural buckling is critical (i.e., $N_{cr,F} < N_{cr,T}$), the post-buckling stability is practically neutral. Note that the highly unstable post-buckling behaviour reported in [8,10] owing to mode interactions when $N_{cr,T}/N_{cr,F} \approx 1.0$ is not observed for flanged cruciform section columns. The aforementioned features of the post-buckling behaviour are confirmed in Fig. 14. Here, the ratio $(\chi - \chi_F)/(\chi_T - \chi_F)$, in which $\chi = N_{u,FE}/Af_y$ is the buckling reduction factor determined from the FE results, χ_T is the torsional buckling reduction factor based on the plate buckling curve specified in EN 1993-1-5 [41] and χ_F is the flexural reduction factor based on the flexural buckling curve specified in EN 1993-1-1 [2], is plotted against various $N_{cr,T}/N_{cr,F}$ values for two sets of columns with the same local slenderness $\bar{\lambda}_L = \sqrt{Af_y/N_{cr,L}}$, which is based on the full cross-sectional elastic local buckling load presented in Section 3, and different member slendernesses $\bar{\lambda}$ or $\bar{\lambda}_T$. Maintaining the local slenderness $\bar{\lambda}_L$ to be the same within each set aims to isolate the effect of member slendernesses on the mechanical behaviour. For low $N_{cr,T}/N_{cr,F}$ values, the $(\chi - \chi_F)/(\chi_T - \chi_F)$ ratio is close to unity, demonstrating that the torsional post-buckling behaviour is stable and approaches the capacity predictions of plates given in EN 1993-1-5 [41]. As $N_{cr,T}/N_{cr,F}$ increases, the $(\chi - \chi_F)/(\chi_T - \chi_F)$ ratio decreases and converges to zero, representing the gradual transition from torsional to flexural buckling, and that for large $N_{cr,T}/N_{cr,F}$ values, torsional deformation diminishes and flexural buckling becomes dominant, so that the buckling reduction factor χ is well predicted by the existing flexural buckling curve given in EN 1993-1-1 [2]. This smooth transition from stable to practically neutral post-buckling behaviour of flanged cruciform columns as the elastic buckling load ratio $N_{cr,T}/N_{cr,F}$ increases can be seen as a benefit, as opposed to many different thin-walled members whose post-buckling behaviour exhibits highly unstable features when the respective buckling loads are relatively close numerically.

It can be seen in Fig. 13(b) that the FE results and analytical solutions from Eq. (17) agree well, with a trivial fundamental path before the critical elastic buckling load is reached, followed by a symmetric and stable post-buckling path; the horizontal plateaus for the FE results represent the transition from stable torsional post-buckling behaviour to almost neutral flexural post-buckling behaviour. The stable torsional post-buckling behaviour is attributed to the shear stresses induced by uniform torsion in open thin-walled sections, which are parallel to the walls of the section and vary linearly through the section thickness [23]. For demonstration purposes, the relationship between the shear to direct stress ratio τ/σ and normalised axial load N/N_{cr}, and normalised axial shortening δ/δ_{cr} for flanged cruciform section columns with $N_{cr,T}/N_{cr,F} = 0.50$ and 2.50 is plotted in Fig. 15. Here, the stress ratio τ/σ is defined as the ratio of the maximum shear stress τ at the critical cross-sections (i.e., the inflexion points where cross-sectional shear stresses are at their maximum along the member length) over the average normal stress σ across the cross-sections. It is observed that for cases where torsional buckling is critical (i.e., $N_{cr,T}/N_{cr,F} = 0.50$), both the normalised load and the normalised axial shortening increase with increasing stress ratios, while for the flexural buckling critical case (i.e., $N_{cr,T}/N_{cr,F} = 2.50$), the normalised load remains at unity and the normalised axial shortening increases with stress ratios remaining at minimal and gradually decreasing values. Since the maximum shear stress values occur in the flanges at the critical cross-sections, the stabilising and strengthening effects of the flanges can be seen as being critically important for providing the stable torsional post-buckling behaviour of flanged cruciform section columns, as opposed to other thin-walled structural members without flanges that are susceptible to torsional buckling, such as fixed-ended equal-leg angle section columns [8] and plain cruciform section columns [10], where unstable post-buckling is sometimes observed.

6. Current design to Eurocode 3

In EN 1993-1-1 [2], flanged cruciform sections can be deemed as Class 1–3, i.e., not susceptible to local buckling before the yield load is reached, based on their constituent I-sections if the following criteria are both satisfied:

$$c_w/t_w \leq 38\epsilon, \quad c_f/t_f \leq 14\epsilon. \tag{18}$$

Here, c_w and c_f are the clear width of the flat regions of the internal (i.e., $c_w = b_w - t_w/2 - t_f/2 - 2r$, where r is the fillet radius) and outstand ($c_f = b_f - t_w/2 - r$) elements, respectively, and $\epsilon = \sqrt{235/f_y}$. The cross-sections beyond these geometric proportion limits fall into the Class 4 category and the effective area A_{eff}, as specified in EN 1993-1-5 [41], is adopted in place of the gross area A. The design member resistance $N_{b,Rd}$ is given in EN 1993-1-1 [2] as:

$$N_{b,Rd} = \frac{\chi A f_y}{\gamma_{M1}}, \tag{19}$$

where A is the gross cross-sectional area, which is replaced by the effective area A_{eff} for Class 4 sections, χ is the member buckling reduction factor associated with the corresponding member buckling curve, and γ_{M1} is the partial safety factor for the member resistance to instability, equal to 1.0 for steel components. The buckling reduction factor χ is given as:

$$\chi = \frac{1}{\phi + \sqrt{\phi^2 - \bar{\lambda}_i^2}} \quad \text{but} \quad \chi \leq 1.0 \tag{20}$$

where $\bar{\lambda}_i$ is the relevant normalised slenderness for torsional (T) or flexural (F) buckling, thus:

$$\bar{\lambda}_i = \sqrt{\frac{Af_y}{N_{cr,i}}} \quad \text{where i=\{T, F\}.} \tag{21}$$

Here, $N_{cr,i}$ is the elastic buckling load for the relevant buckling mode, and A is replaced by the effective area A_{eff} for Class 4 sections; ϕ is an auxiliary parameter defined as:

$$\phi = 0.5\left[1 + \eta + \bar{\lambda}_i^2\right] \tag{22}$$

where η is the generalised initial imperfection factor given as:

$$\eta = \alpha(\bar{\lambda}_i - \bar{\lambda}_0), \tag{23}$$

and α is the imperfection factor while $\bar{\lambda}_0$ is the limiting slenderness. Since there is no guidance in EN 1993-1-1 [2] on the choice of the imperfection factor α value specifically for flanged cruciform sections, and considering the similarities in the manufacturing process between flanged cruciform sections and welded I-sections, the corresponding buckling curve 'c', where $\alpha = 0.49$, is assumed herein, and the limiting slenderness $\bar{\lambda}_0$ is taken as 0.2. Comparisons of the ultimate loads collected from the FE and test results with the resistances calculated from EC3, $N_{b,EC3}$, are presented in Table 6 and Fig. 16, for cases with torsional buckling being critical (i.e., $N_{cr,T} \leq N_{cr,F}$) and flexural buckling being critical (i.e., $N_{cr,F} < N_{cr,T}$). A high level of conservatism is clearly observed for cases where torsional buckling is critical,

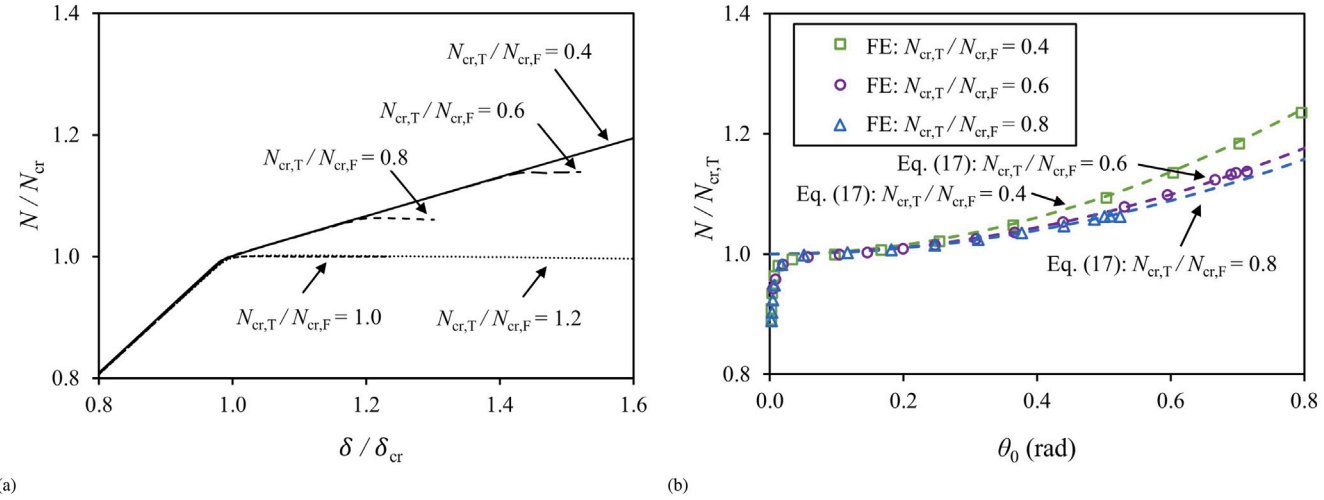

Fig. 13. Relationship between normalised axial load N/N_{cr} and (a) normalised axial shortening δ/δ_{cr} from the FE results, and (b) angle of twist at member mid-height θ_0 from the FE results and Eq. (17) for cases where torsional buckling is critical (i.e., $N_{cr,T} \le N_{cr,F}$) for flanged cruciform section columns with the same member slenderness $\bar{\lambda}_T$ or $\bar{\lambda}$.

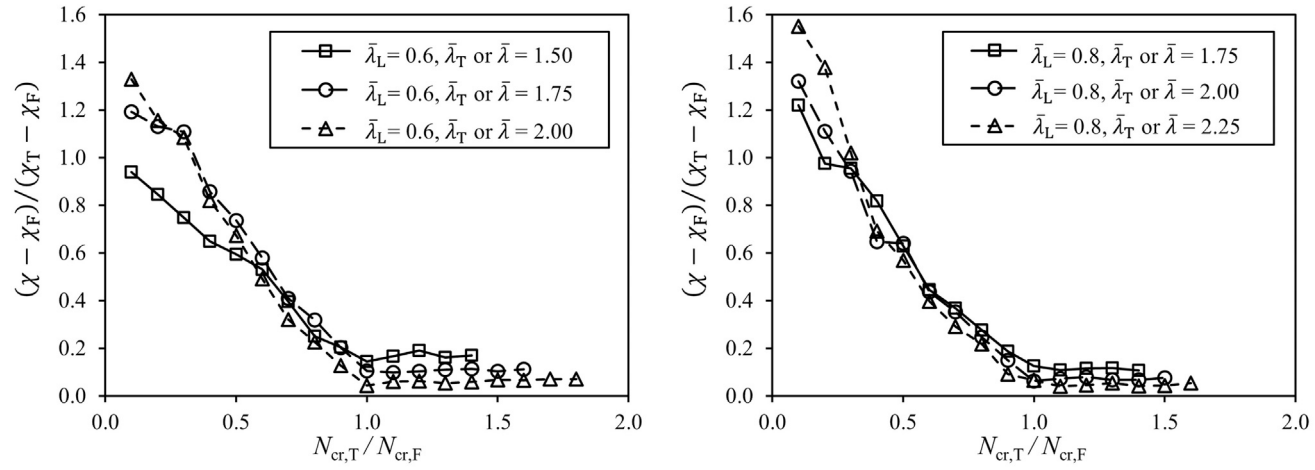

Fig. 14. Relationship between $(\chi - \chi_F)/(\chi_T - \chi_F)$ and $N_{cr,T}/N_{cr,F}$ for flanged cruciform section columns with (a) $\bar{\lambda}_L = 0.6$ and (b) $\bar{\lambda}_L = 0.8$, where $\bar{\lambda}_L = \sqrt{Af_y/N_{cr,L}}$.

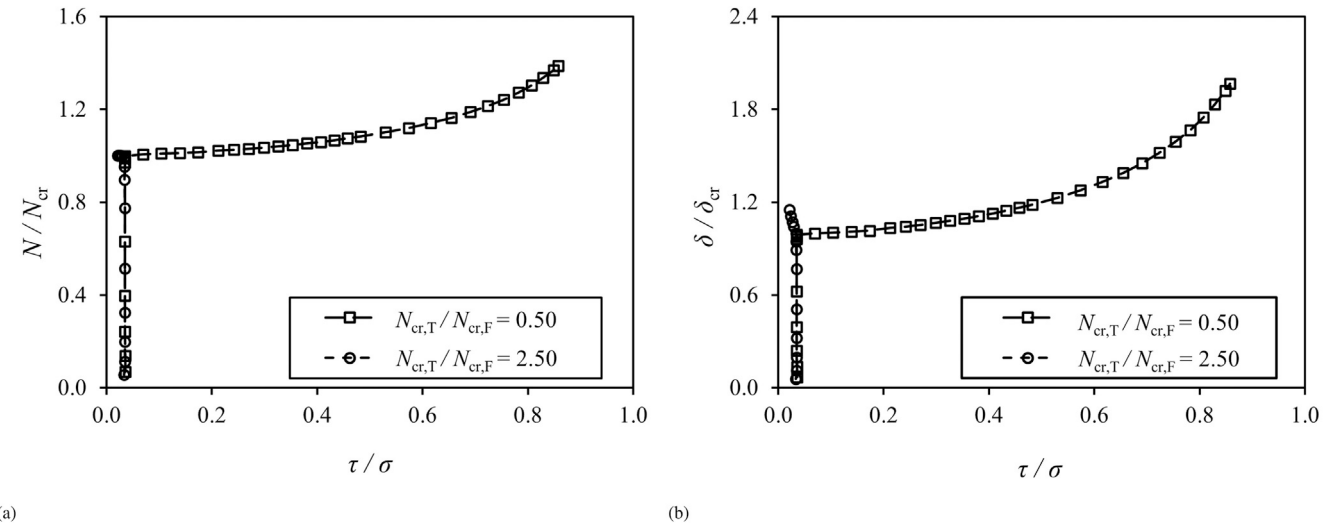

Fig. 15. Relationship between the shear to direct stress ratio τ/σ and (a) normalised axial load N/N_{cr}, and (b) normalised axial shortening δ/δ_{cr} for flanged cruciform section columns with $N_{cr,T}/N_{cr,F} = 0.50$ and 2.50.

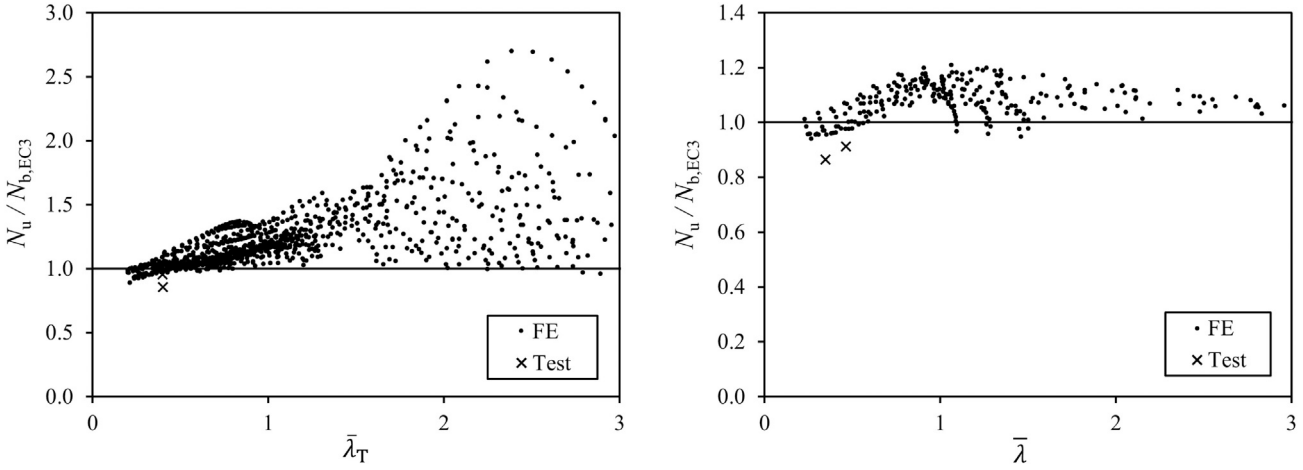

Fig. 16. Comparisons of the ultimate resistances collected from FE and test results alongside predictions from EC3 for flanged cruciform section columns for cases where (a) torsional buckling is critical (i.e., $N_{cr,T} \leq N_{cr,F}$) with $\bar{\lambda}_T = \sqrt{Af_y/N_{cr,T}}$ and $A = A_{eff}$ for Class 4 sections, and (b) flexural buckling is critical (i.e., $N_{cr,F} < N_{cr,T}$) with $\bar{\lambda} = \sqrt{Af_y/N_{cr,F}}$ and $A = A_{eff}$ for Class 4 sections.

Table 6
Summary of comparisons between the ultimate resistances collected from the FE and test results and those predicted using EC3 approach for flanged cruciform section columns.

Source	Evaluation parameter	$N_u/N_{b,EC3}$		
		Torsional	Flexural	Total
FE	Mean	1.25	1.07	1.21
	CoV	0.20	0.05	0.20
Tests	Mean	0.93	0.91	0.92
	CoV	0.05	0.03	0.04

in particular for members with large normalised slendernesses. This phenomenon can be attributed to the earlier finding that the stable post-buckling response, observed when torsional buckling is clearly critical, is significantly underestimated by the flexural buckling curve, which is predicated on an almost neutral post-buckling response. The European design code for aluminium alloy structures EN 1999-1-1 [49] provides different buckling curves for flexural and torsional buckling critical cases. The present aim is to resolve this apparent inconsistency within the Eurocode design guidance by proposing a new design approach to predict the ultimate resistance of flanged cruciform section columns more accurately.

7. New design proposals

To resolve the aforementioned drawbacks and inconsistencies in the present Eurocode, new design proposals for flanged cruciform section columns are presented and subsequently assessed based on the observations in Section 5, following similar procedures to those developed in [8–10].

7.1. New proposal for torsional buckling

In order to represent the vertical scattering of the buckling reduction factor χ at the same $\bar{\lambda}_T$ with different $N_{cr,T}/N_{cr,F}$ ratios, modifications to the upper bound were first made since torsional buckling and local buckling are no longer the same mode for flanged cruciform section columns unlike the cases of fixed-ended equal-leg angle section columns [8] and plain cruciform columns [10]. The newly proposed curve is to be adopted for both the upper bound for torsional buckling (Fig. 9b) and local buckling of the constituent plates (Fig. 9c). Hence, the upper bound for the torsional buckling reduction factor χ_T is given thus:

$$\chi_T = 1.0 \quad \text{for} \quad \bar{\lambda}_T \leq 0.550,$$
$$\chi_T = \frac{\bar{\lambda}_T - 0.248}{\bar{\lambda}_T^2} \leq 1.0 \quad \text{for} \quad \bar{\lambda}_T > 0.550. \tag{24}$$

This upper bound corresponds to the cases where torsional buckling is dominant, i.e., $N_{cr,T}/N_{cr,F} \to 0$. The plate buckling reduction factor, applied to Class 4 cross-sections, ρ, is determined thus:

$$\rho = 1.0 \quad \text{for} \quad \bar{\lambda}_p \leq 0.550,$$
$$\rho = \frac{\bar{\lambda}_p - 0.248}{\bar{\lambda}_p^2} \leq 1.0 \quad \text{for} \quad \bar{\lambda}_p > 0.550, \tag{25}$$

Here, $\bar{\lambda}_p = \sqrt{f_y/\sigma_{cr,p}}$, where $\sigma_{cr,p}$ is given by Eq. (10). The formulae are to be applied to both the flanges and the webs that fall into the Class 4 category; the corresponding Class 4 slenderness limits are $c_w/t_w \leq 31.2\epsilon$ for webs and $c_f/t_f \leq 10.2\epsilon$ for outstand flanges. The effective areas A_{eff} of flat compression elements can be obtained with the relationship $A_{eff} = \rho A$. Note that the overall effective area of the cross-section is determined based on the individual isolated plate elements, as opposed to the full cross-sectional elastic local buckling load $N_{cr,L}$ developed in Section 3; this is to ensure alignment with the current EC3 design provisions [2,41]. This newly proposed curve is determined such that it bears a resemblance to the existing plate buckling curves given in EN 1993-1-5 [41] and it captures an upper bound envelope of the FE results. Note that the coefficients in the proposed formulae for torsional buckling are determined based on the numerical results of flanged cruciform section columns; these coefficients are therefore subject to further modifications for other scenarios. This argument is similar to the choice of imperfection factor α for the flexural buckling curves in EN 1993-1-1 [2], which is determined on a case-by-case basis for different cross-sectional types, geometric proportions, manufacturing methods and the axes about which buckling occurs.

A comparison between the newly proposed torsional buckling curve, the existing plate buckling curves for outstand and internal elements in EN 1993-1-5 [41] and the flexural buckling curve in EN 1993-1-1 [2] is presented in Fig. 17. Through the employment of the newly proposed torsional buckling upper bound, the FE data points related to Class 4 sections shift upwards and to the right, as shown in Fig. 18, corresponding to the decreased effective area A_{eff} compared to those produced with the existing plate buckling curves in EN 1993-1-5 [41].

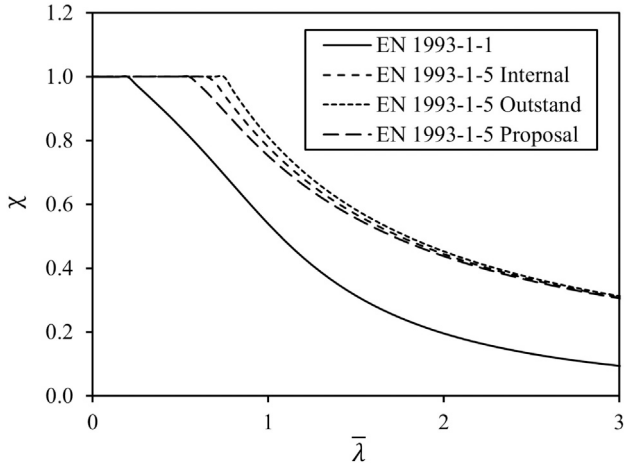

Fig. 17. Relationship between the newly proposed torsional buckling curve with the existing plate buckling curves for outstand and internal elements in EN 1993-1-5 [41] and the flexural buckling curve in EN 1993-1-1 [2].

The FE results produced from the parametric studies are presented in Fig. 18 in the form of the reduction factor χ against the normalised slenderness, with the newly proposed torsional buckling curve and the flexural buckling curve from EN 1993-1-1 [2] serving as the upper and lower boundaries, respectively. These bounds provide a clearly improved representation of the data spread compared to those shown in Fig. 12, considering in particular Fig. 18(a) versus Fig. 12(a). This improvement enables the employment of the design approach developed in recent studies [8–10]. Hereinafter, a new parameter Δ_F is introduced to capture the variation of the buckling reduction factor χ between the newly proposed upper bound and the existing lower bound with different $N_{cr,T}/N_{cr,F}$ ratios, defined as:

$$\Delta_F = \frac{\chi - \chi_F}{\chi_T - \chi_F} \tag{26}$$

where χ_T is the torsional buckling reduction factor based on the newly proposed torsional buckling upper bound, while χ and χ_F are previously defined for Fig. 14 in Section 5. The definitions of $(\chi - \chi_F)$ and $(\chi_T - \chi_F)$ are demonstrated in Fig. 19, where the solid point represents the buckling reduction factor of one specific flanged cruciform section column. The numerical results for Δ_F from the FE parametric studies are plotted against the $N_{cr,T}/N_{cr,F}$ ratio in Fig. 20; and a selection of numerical results with three typical normalised slendernesses $\bar{\lambda}_T$ are presented for demonstration purposes. It is observed that Δ_F decreases with increasing $N_{cr,T}/N_{cr,F}$ and this trend is more prominent for a certain range of $\bar{\lambda}_T$ values. This trend is captured through the following equation for determining Δ_F:

$$\Delta_F = \left(1 - \frac{N_{cr,T}}{N_{cr,F}}\right)^p \tag{27}$$

where the term in the parentheses captures the relationship between Δ_F and $N_{cr,T}/N_{cr,F}$ while the power p is determined thus:

$$p = 2.73\bar{\lambda}_T^{-2.5}, \quad \text{but} \quad 1.2 \le p \le 10.0. \tag{28}$$

Here, the coefficients and limiting values in the formulae were determined such that the trend of the relationship between Δ_F and $N_{cr,T}/N_{cr,F}$ with respect to $\bar{\lambda}_T$ was captured. From Fig. 20, it can be seen that the proposed formula, Eq. (27), is able to capture the trend of the FE results well, at least as lower bounds. The theoretical upper bound $\Delta_F = 1.0$ represents pure torsional buckling when $N_{cr,T}/N_{cr,F} \to 0$, while the theoretical lower bound $\Delta_F = 0$, corresponding to flexural buckling, is reached when $N_{cr,T}/N_{cr,F} = 1$. The predicted buckling reduction factor χ can be determined using linear interpolation by rearranging Eq. (26), thus:

$$\chi = \chi_F + \Delta_F\,(\chi_T - \chi_F). \tag{29}$$

A comparison between a selection of FE results and the new design proposals for three typical $N_{cr,T}/N_{cr,F}$ ratios is presented in Fig. 21 in the form of the buckling reduction factor χ against the normalised slenderness $\bar{\lambda}_T$, where good agreement is observed between the numerical results and their predictive counterparts. The proposed design resistance for flanged cruciform section columns for cases where torsional buckling is critical (i.e., $N_{cr,T} \le N_{cr,F}$) is hence determined as:

$$N_{b,Rd} = \frac{\chi A f_y}{\gamma_{M1}} \tag{30}$$

where, as before, the gross cross-sectional area A is substituted by the effective area A_{eff} for Class 4 sections. Note that in previous studies for fixed-ended equal-leg angle section columns [8,9] and plain cruciform section columns [10], it was proposed to use the gross cross-sectional area A for Class 4 sections when torsional buckling is critical (i.e.,

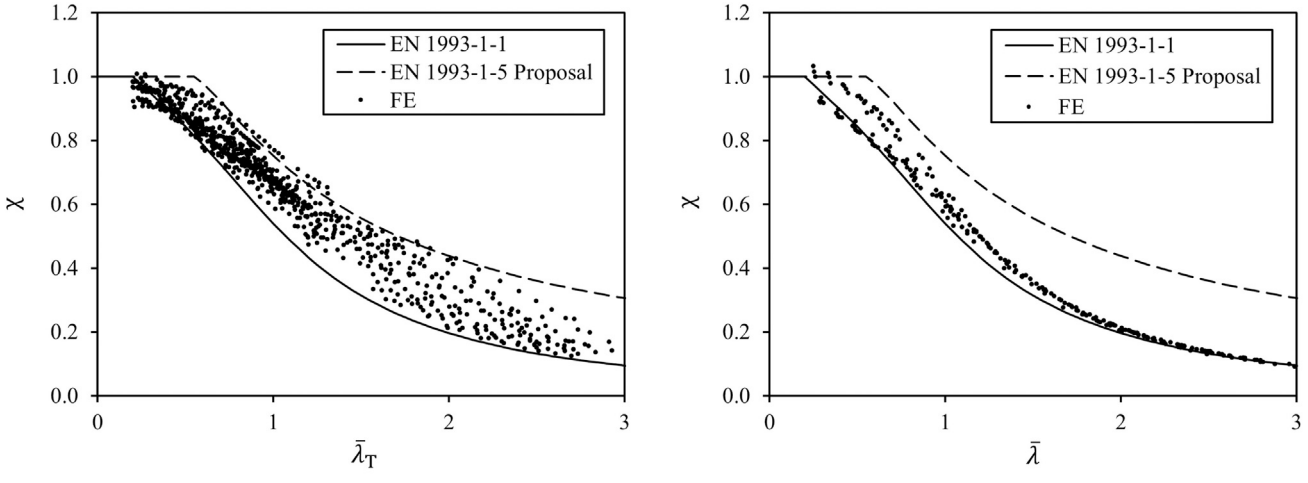

Fig. 18. Comparison of FE results for spherically-pinned steel flanged cruciform section columns against the newly proposed torsional buckling curve and the flexural buckling curve in EN 1993-1-1 [2], where: (a) torsional buckling is critical (i.e., $N_{cr,T} \le N_{cr,F}$) with $\bar{\lambda}_T = \sqrt{Af_y/N_{cr,T}}$ and $A = A_{eff}$ for Class 4 sections, and (b) flexural buckling is critical (i.e., $N_{cr,F} < N_{cr,T}$) with $\bar{\lambda} = \sqrt{Af_y/N_{cr,F}}$ and $A = A_{eff}$ for Class 4 sections.

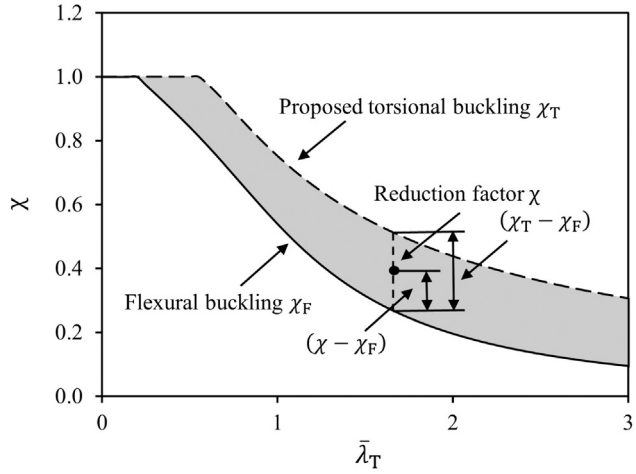

Fig. 19. Demonstration of $(\chi - \chi_F)$ and $(\chi_T - \chi_F)$ that are employed to determine Δ_F.

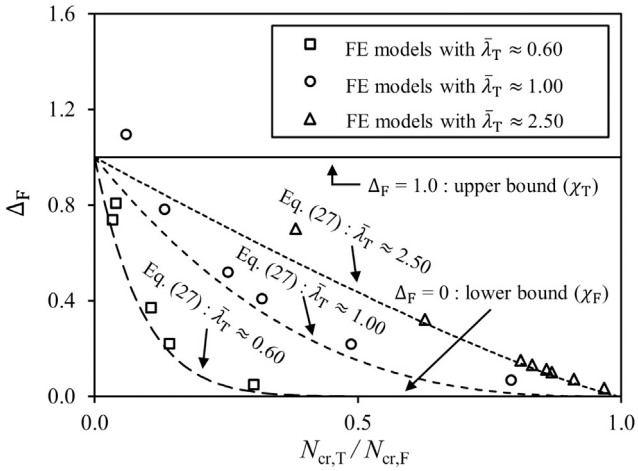

Fig. 20. Parameter Δ_F from FE results and proposed formulae against $N_{cr,T}/N_{cr,F}$ for flanged cruciform section columns.

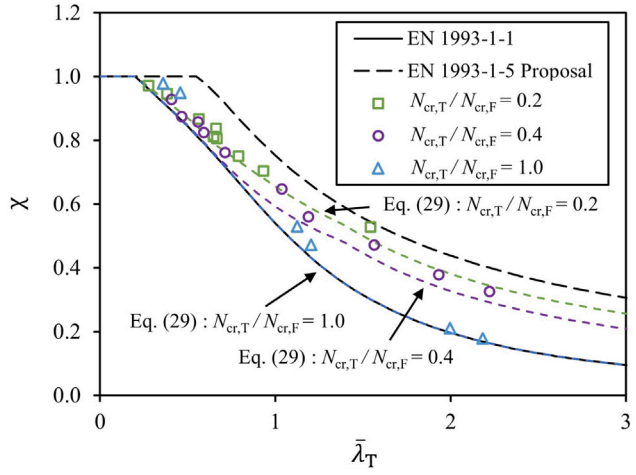

Fig. 21. Comparisons between FE results and new design proposals with three typical $N_{cr,T}/N_{cr,F}$ ratios in the form of χ against $\bar{\lambda}_T$ for flanged cruciform section columns.

$N_{cr,T} \leq N_{cr,F}$). This approach was derived from the finding that torsional buckling and local buckling are essentially the same mode for the aforementioned cross-sections, and thus avoids the same phenomenon being accounted for twice. However, in the present context of flanged cruciform section columns, torsional and local buckling are no longer the same; hence the use of the effective area A_{eff} is maintained.

Table 7
Summary of comparisons between the ultimate resistances collected from the FE and test results and those predicted using the new design proposals for flanged cruciform section columns.

Source	Evaluation parameter	$N_u/N_{b,prop}$		
		Torsional	Flexural	Total
FE	Mean	1.07	1.07	1.07
	CoV	0.07	0.05	0.06
Tests	Mean	0.96	0.94	0.95
	CoV	0.01	0.01	0.01

7.2. New proposal for flexural buckling

In previous studies [8–10], the newly proposed flexural buckling design approach featured the introduction of a factor β to the generalised initial imperfection factor η to represent the influence of mode interaction. However, as stated in Section 5, significant interactions between torsional and flexural buckling modes were not observed for flanged cruciform section columns; introduction of this factor is therefore unnecessary herein. Moreover, it can be seen in Figs. 12(b) and 18(b) that the existing flexural buckling curve in EN 1993-1-1 [2] provides accurate and generally slightly safe-sided resistance predictions for the FE results; therefore, the existing flexural buckling curve with the imperfection factor $\alpha = 0.49$ and $\bar{\lambda}_0 = 0.2$ is deemed to be appropriate for predicting the ultimate resistance of flanged cruciform section columns where flexural buckling is critical (i.e., $N_{cr,F} < N_{cr,T}$). In order to achieve consistency in resistance predictions at the transition point (i.e., $N_{cr,T}/N_{cr,F} = 1$), it is proposed to use the torsional buckling upper bound specified in Section 7.1 to calculate the effective area A_{eff} for Class 4 flanged cruciform sections.

7.3. Assessment of new design proposals

A summary of the comparisons between the ultimate resistances collected from the FE and test results and those predicted using the new design proposals for flanged cruciform section columns is presented in Table 7 and Fig. 22. By comparing Fig. 22(a) against Fig. 16(a), a remarkable improvement is observed in resistance predictions since the new design proposal solves the problem of over conservatism in EC3 for cases where torsional buckling is critical (i.e., $N_{cr,T} \leq N_{cr,F}$). By comparing Fig. 22(b) against Fig. 16(b), no significant differences can be seen, since the existing flexural buckling curve already captures the resistance well for cases where flexural buckling is critical (i.e., $N_{cr,F} < N_{cr,T}$), yet the new proposal refines the predictions for a few particular cases.

7.4. Reliability analysis

A reliability analysis of the current EN 1993-1-1 [2] and newly proposed design approaches for flanged cruciform section columns is performed following the standard procedures specified in EN 1990 [50]. The variability of material properties and geometric dimensions was first determined in accordance with Annex E of EN 1993-1-1 [2]. Since there is no guidance specifically provided for flanged cruciform sections, the suggested values for the constituent I-sections were adopted herein, as presented in Table 8, where X_m/X_n denotes the ratio of the mean over the nominal values of a property X and V_X is the corresponding coefficient of variation (CoV). The mean and CoV of the material properties, Young's modulus E and yield strength f_y for

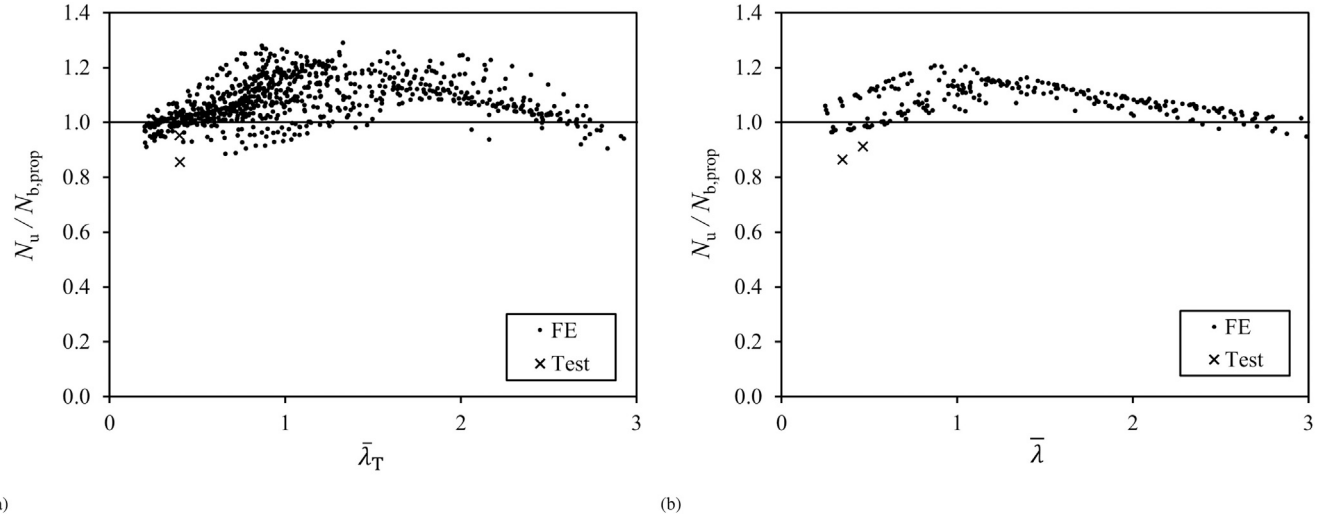

Fig. 22. Comparisons of the ultimate resistances collected from FE and test results alongside predictions from the new design proposals for flanged cruciform section columns for cases where (a) torsional buckling is critical (i.e., $N_{cr,T} \leq N_{cr,F}$) with $\bar{\lambda}_T = \sqrt{Af_y/N_{cr,T}}$ and $A = A_{eff}$ for Class 4 sections, and (b) flexural buckling is critical (i.e., $N_{cr,F} < N_{cr,T}$) with $\bar{\lambda} = \sqrt{Af_y/N_{cr,F}}$ and $A = A_{eff}$ for Class 4 sections.

Table 8
Mean and CoV values of material properties and geometric dimensions for flanged cruciform sections based on constituent I-sections in accordance with Annex E of EN 1993-1-1 [2].

Parameter	X_m/X_n	V_X
E	1.00	0.030
f_y (S355)	1.20	0.050
h	1.00	0.009
b	1.00	0.009
t_w	1.00	0.025
t_f	0.98	0.025

S355 steel, were taken as specified in Table 8 according to EN 1993-1-1 [2]. The CoV of the cross-sectional area V_A, representing the overall variability of the cross-sectional dimensions, was calculated based on the individual geometric components listed in Table 8, following the procedure described in [51]. The individual V_A varies slightly across cross-sectional profiles while an average value of $V_A = 0.020$ was adopted herein.

The design column resistance can be expressed in a general form [52] in terms of the basic variables comprising the yield strength f_y, the cross-sectional area A and the Young's modulus E, as described thus:

$$N_{b,Rd} = k f_y{}^c A^d E^e, \tag{31}$$

where k is the model constant, while c, d and e are model parameters that represent the dependency of the member resistance on their corresponding basic variables. The values of the model parameters were calculated individually for each experiment and numerical simulation following the approach described in [51]. The combined CoV of the material properties and geometric dimensions, namely f_y, E and A, was then calculated using the following equation:

$$V_{rt} = \sqrt{(cV_{f_y})^2 + (dV_A)^2 + (eV_E)^2}. \tag{32}$$

The CoV of the test and FE resistances relative to the design predictions V_δ, the combined CoV, incorporating the variability of the resistance model and the basic variables, V_r, and the design fractile factor $k_{d,n}$ were calculated in accordance with EN 1990 [50]. Note that the correction factor b was determined thus:

$$b = \frac{1}{n}\sum_{i=1}^{n}\frac{r_{e,i}}{r_{t,i}} \tag{33}$$

where n is the population of test and FE data, r_e is the experimental or FE resistance and r_t is the theoretical resistance determined from the prediction model. This was used in place of the least squares approach specified in EN 1990 [50]. This approach prevents the b value being biased towards the test and FE samples with higher resistance values [31].

The test and FE data were first divided into two groups based on the critical buckling mode (i.e., torsional or flexural buckling), and subsequently subdivided at the normalised slenderness of $\bar{\lambda}_T = 1.50$ and $\bar{\lambda} = 1.25$, respectively, in order not to overestimate the scattering of the data. The key reliability analysis results are reported in Tables 9 and 10 for the current EC3 and proposed design approach, respectively, where γ^*_{M1} is the required value of the partial safety factor, determined following the procedures described in [51], γ_{M1} is the target value of the partial safety factor, taken as 1.0, and f_a is the acceptance limit recommended in [53] as:

$$f_a = 1.03 + 0.75(V_r - 0.04) \quad \text{and} \quad 1.03 \leq f_a \leq 1.15. \tag{34}$$

The $\gamma^*_{M1}/\gamma_{M1}$ ratios should satisfy the following relationship:

$$\gamma^*_{M1}/\gamma_{M1} \leq f_a \tag{35}$$

for the corresponding design approach to be deemed acceptable. The current EC3 design approach leads to excessively high $(\gamma^*_{M1}/\gamma_{M1})/f_a$ values, in particular when torsional buckling is critical, as shown in Table 9, mainly owing to the over conservatism in the torsional strength predictions. The proposed design approach yields $(\gamma^*_{M1}/\gamma_{M1})/f_a$ values of 1.006 and 1.005 for the cases in which torsional and flexural buckling were critical, respectively, as shown in Table 10, which are deemed acceptable. A graphical comparison of the $\gamma^*_{M1}/\gamma_{M1}$ ratios with the acceptance limit f_a recommended in [53] is plotted for the proposed design approach in Fig. 23.

8. Conclusions

A comprehensive study into steel flanged cruciform section members subjected to axial compression has been presented. Numerical models were established and validated against existing experimental results reported in the literature; good agreement was observed between the FE and test responses. A parametric study was subsequently conducted covering a wide spectrum of cross-sectional geometric proportions, normalised slendernesses and elastic buckling load

Table 9
Reliability analysis results for the present EC3 design approach.

Source	Critical buckling mode	$k_{d,n}$	b	V_δ	V_r	γ^*_{M1}	$\gamma^*_{M1}/\gamma_{M1}$	f_a	$(\gamma^*_{M1}/\gamma_{M1})/f_a$
FE and Test	Torsional	3.101	1.244	0.189	0.195	1.355	1.355	1.146	1.183
	Flexural	3.130	1.067	0.050	0.064	1.083	1.083	1.048	1.034

Table 10
Reliability analysis results for currently proposed design approach.

Source	Critical buckling mode	$k_{d,n}$	b	V_δ	V_r	γ^*_{M1}	$\gamma^*_{M1}/\gamma_{M1}$	f_a	$(\gamma^*_{M1}/\gamma_{M1})/f_a$
FE and Test	Torsional	3.101	1.073	0.075	0.090	1.074	1.074	1.068	1.006
	Flexural	3.130	1.063	0.062	0.074	1.061	1.061	1.055	1.005

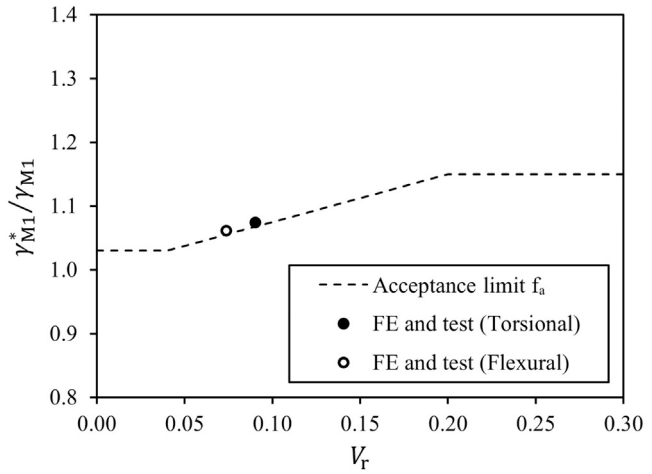

Fig. 23. Comparison of the $\gamma^*_{M1}/\gamma_{M1}$ ratios with the acceptance limit f_a for the proposed design approach.

ratios. The parametric study and existing test results were then employed to assess the current EC3 design guidance for steel flanged cruciform section columns. Both torsional and flexural instabilities are treated as member-level buckling modes (utilising the same buckling curve) within the current EC3 design provisions for flanged cruciform section columns. However, it has been revealed within the current study that, for members with the same torsional normalised slenderness $\bar{\lambda}_T$, the buckling behaviour can vary significantly with different elastic buckling load ratios $N_{cr,T}/N_{cr,F}$; this variation is principally attributed to the differing post-buckling responses associated with different $N_{cr,T}/N_{cr,F}$ ratios. For flanged cruciform section column members with low $N_{cr,T}/N_{cr,F}$ ratios, torsional buckling governs and the corresponding post-buckling response is strongly stable; for members with $N_{cr,T}/N_{cr,F}$ ratios close to unity, the critical mode transitions from torsional to flexural buckling; for members with high $N_{cr,T}/N_{cr,F}$ ratios, flexural buckling becomes dominant and the corresponding post-buckling response is practically neutral. A new design approach has been proposed for flanged cruciform section columns, inspired by recent research on fixed-ended equal-leg angle section columns and plain cruciform section columns. The proposed design approach has introduced a new parameter Δ_F to capture the aforementioned variation in post-buckling behaviour and ultimate resistance for members with the same torsional slenderness $\bar{\lambda}_T$ but varying $N_{cr,T}/N_{cr,F}$ ratios. The proposed design approach has been shown to provide significant improvements in the accuracy and reliability of the ultimate resistance predictions of flanged cruciform section columns compared with the current EC3 design provisions.

CRediT authorship contribution statement

Ruikai Dai: Writing – original draft, Software, Methodology, Investigation, Formal analysis, Conceptualization. **Behnam Behzadi-Sofiani:** Methodology, Investigation, Formal analysis, Conceptualization. **Spiridione Buhagiar:** Investigation, Conceptualization. **M. Ahmer Wadee:** Writing – review & editing, Supervision, Resources, Methodology, Investigation, Conceptualization. **Leroy Gardner:** Writing – review & editing, Supervision, Resources, Methodology, Investigation, Formal analysis, Conceptualization.

Declaration of competing interest

The authors declare the following financial interests/personal relationships which may be considered as potential competing interests: M. Ahmer Wadee is Editor of Thin-Walled Structures and Leroy Gardner serves on the Editorial Board of Thin-Walled Structures. If there are other authors, they declare that they have no known competing financial interests or personal relationships that could have appeared to influence the work reported in this paper.

Data availability

Data will be made available on request.

Acknowledgements

The authors gratefully acknowledge the Skempton scholarship from Imperial College London, United Kingdom and the funding from the China Scholarship Council for the financial support for the lead author.

References

[1] N. Harris, G. Urgessa, Strength of flanged and plain cruciform members, Adv. Civil Eng. 2018 (2018) 1–7.
[2] EN 1993-1-1, Eurocode 3: Design of steel structures – Part 1-1: General rules and rules for buildings, European Committee for Standardisation (CEN), Brussels, Belgium, 2022.
[3] AISC, Specification for structural steel buildings, American Institute of Steel Construction, Chicago, IL, USA, 2016.
[4] P.B. Dinis, D. Camotim, N. Silvestre, Post-buckling behaviour and strength of angle columns, in: Proc., Int. Colloquium on Stability and Ductility of Steel Structures, SDSS, Federal Univ. of Rio de Janeiro and State Univ. of Rio de Janeiro, Rio de Janeiro, 2010, pp. 1141–1150.
[5] P.B. Dinis, D. Camotim, N. Silvestre, On the mechanics of thin-walled angle column instability, Thin-Walled Struct. 52 (2012) 80–89.
[6] N. Silvestre, P.B. Dinis, D. Camotim, Developments on the design of cold-formed steel angles, J. Struct. Eng. 139 (5) (2013) 680–694.
[7] P.B. Dinis, D. Camotim, A novel DSM-based approach for the rational design of fixed-ended and pin-ended short-to-intermediate thin-walled angle columns, Thin-Walled Struct. 87 (2015) 158–182.
[8] B. Behzadi-Sofiani, L. Gardner, M.A. Wadee, P.B. Dinis, D. Camotim, Behaviour and design of fixed-ended steel equal-leg angle section columns, J. Constr. Steel Res. 182 (2021) 106649.
[9] B. Behzadi-Sofiani, L. Gardner, M.A. Wadee, Stability and design of fixed-ended stainless steel equal-leg angle section compression members, Eng. Struct. 249 (2021) 113281.
[10] B. Behzadi-Sofiani, L. Gardner, M.A. Wadee, Behaviour, finite element modelling and design of cruciform section steel columns, Thin-Walled Struct. 182 (2023) 110124.
[11] ABAQUS, Version 6.16 Analysis User's Guide, Providence, RI, USA, Dassault Systemes Simulia Corporation, 2016.

[12] M.M. Tahir, P. Shek, Performance of cruciform column using universal beam sections under axial compression load, J. Teknol. 43 (2005) 51–66.
[13] BS 5950-1, Structural use of steelwork in building – Part 1: Code of practice for design – Rolled and welded sections, British Standards Institution, London, United Kingdom, 2000.
[14] M.M. Tahir, P.N. Shek, A. Sulaiman, C.S. Tan, Experimental investigation of short cruciform columns using universal beam sections, Constr. Build. Mater. 23 (3) (2009) 1354–1364.
[15] J. Dobrić, N. Fric, E. Naraidoo, B. Rossi, Experimental behaviour of cold-formed stainless steel cruciform section columns, ce/papers 6 (3–4) (2023) 655–659.
[16] B.K. Kiani, S. Torabian, S.R. Mirghaderi, Local seismic stability of flanged cruciform sections (FCSs), Eng. Struct. 96 (2015) 126–138.
[17] M.M. Nasrabadi, S. Torabian, S.R. Mirghaderi, Panel zone modelling of flanged cruciform columns: An analytical and numerical approach, Eng. Struct. 49 (2013) 491–507.
[18] H. Saffari, S. Sarfarazi, A. Fakhraddini, A mathematical steel panel zone model for flanged cruciform columns, Steel Compos. Struct. 20 (4) (2016) 851–867.
[19] S. Sarfarazi, H. Saffari, A. Fakhraddini, Shear behavior of panel zone considering axial force for flanged cruciform columns, Civil Eng. Infrastruct. J. 53 (2) (2020) 359–377.
[20] S.E. Svensson, C.M. Plum, Stiffener effects on torsional buckling of columns, J. Struct. Eng. 109 (3) (1983) 758–772.
[21] C. King, Design of cruciform sections using BS 5950-1: 2000, New Steel Construct. 14 (4) (2006) 30–32.
[22] S.P. Timoshenko, J.M. Gere, Theory of elastic stability, Second Edition, McGraw-Hill Book Company, Inc., New York and London, 1961.
[23] N.S. Trahair, M. Bradford, D.A. Nethercot, L. Gardner, The behaviour and design of steel structures to EC3, CRC Press, 2017.
[24] L. Gardner, A. Fieber, L. Macorini, Formulae for calculating elastic local buckling stresses of full structural cross-sections, Structures 17 (2019) 2–20.
[25] L. Gardner, X. Yun, F. Walport, The continuous strength method – review and outlook, Eng. Struct. 275 (2023) 114924.
[26] B.W. Schafer, S. Adany, Buckling analysis of cold-formed steel members using CUFSM: conventional and constrained finite strip methods, in: Eighteenth International Specialty Conference on Cold-Formed Steel Structures, Citeseer, 2006, pp. 39–54.
[27] Z. Li, B.W. Schafer, Buckling analysis of cold-formed steel members with general boundary conditions using CUFSM conventional and constrained finite strip methods, Missouri University of Science and Technology, 2010.
[28] F. Bleich, Buckling strength of metal structures, McGraw-Hill Book Company, Inc., New York, 1952.
[29] P.S. Bulson, The stability of flat plates, Chatto and Windus, London, 1970.
[30] H.G. Allen, P.S. Bulson, Background to buckling, McGraw-Hill Book Company, Inc., London, 1980.
[31] Y. Liang, O. Zhao, Y.L. Long, L. Gardner, Stainless steel channel sections under combined compression and minor axis bending – Part 1: Experimental study and numerical modelling, J. Constr. Steel Res. 152 (2019) 154–161.
[32] M. Kucukler, L. Gardner, L. Macorini, Lateral–torsional buckling assessment of steel beams through a stiffness reduction method, J. Constr. Steel Res. 109 (2015) 87–100.
[33] M. Kucukler, Z. Xing, L. Gardner, Behaviour and design of stainless steel I-section columns in fire, J. Constr. Steel Res. 165 (2020) 105890.
[34] X. Meng, L. Gardner, Cross-sectional behaviour of cold-formed high strength steel circular hollow sections, Thin-Walled Struct. 156 (2020) 106822.
[35] E. Riks, An incremental approach to the solution of snapping and buckling problems, Int. J. Solids Struct. 15 (7) (1979) 529–551.
[36] X. Yun, L. Gardner, Stress-strain curves for hot-rolled steels, J. Constr. Steel Res. 133 (2017) 36–46.
[37] L. Gardner, X. Yun, Description of stress-strain curves for cold-formed steels, Constr. Build. Mater. 189 (2018) 527–538.
[38] R. Cruise, L. Gardner, Residual stress analysis of structural stainless steel sections, J. Constr. Steel Res. 64 (3) (2008) 352–366.
[39] T. Yabuki, J.J. Chambers, Y. Arizumi, T. Shimozato, H. Matsushita, Buckling capacity of welded stainless steel flanges by finite element analysis, Eng. Struct. 49 (2013) 831–839.
[40] H. Yuan, Y. Wang, L. Gardner, Y. Shi, Local–overall interactive buckling of welded stainless steel box section compression members, Eng. Struct. 67 (2014) 62–76.
[41] EN 1993-1-5, Eurocode 3: Design of steel structures – Part 1-5: Plated structural elements, European Committee for Standardisation (CEN), Brussels, Belgium, 2006.
[42] A. Fieber, L. Gardner, L. Macorini, Formulae for determining elastic local buckling half-wavelengths of structural steel cross-sections, J. Constr. Steel Res. 159 (2019) 493–506.
[43] L. Gardner, D.A. Nethercot, Designers' Guide to EN 1993-1-1: Eurocode 3: Design of Steel Buildings, Thomas Telford Publishing, London, 2005.
[44] K.J. Rasmussen, Design of angle columns with locally unstable legs, J. Struct. Eng. 131 (10) (2005) 1553–1560.
[45] V.Z. Vlasov, Thin-walled elastic beams, PST Catalogue 428 (1959).
[46] C. Szymczak, Buckling and initial post-buckling behaviour of thin-walled I columns, Comput. Struct. 11 (6) (1980) 481–487.
[47] F. Mohri, L. Azrar, M. Potier-Ferry, Flexural-torsional post-buckling analysis of thin-walled elements with open sections, Thin-Walled Struct. 39 (11) (2001) 907–938.
[48] N.S. Trahair, Flexural-torsional buckling of structures, CRC Press, 2017.
[49] EN 1999-1-1, Eurocode 9: Design of aluminium structures – Part 1-1: General structural rules, European Committee for Standardisation (CEN), Brussels, Belgium, 2007.
[50] EN 1990, Eurocode – Basis of structural design, European Committee for Standardisation (CEN), Brussels, Belgium, 2005.
[51] S. Afshan, P. Francis, N. Baddoo, L. Gardner, Reliability analysis of structural stainless steel design provisions, J. Constr. Steel Res. 114 (2015) 293–304.
[52] F. Walport, L. Gardner, D. Nethercot, Equivalent bow imperfections for use in design by second order inelastic analysis, Structures 26 (2020) 670–685.
[53] L.S. da Silva, T. Tankova, L. Marques, C. Rebelo, A. Taras, Standardisation of safety assessment procedures across brittle to ductile failure modes (safebrictile), 2018, European Commission, Directorate-General for Research and Innovation, final document.